Alluvial records of the African Humid Period from the NW African highlands (Moulouya basin, NE Morocco)

Bruno Depreux, David Lefèvre, Jean-François Berger, Fatima Segaoui, Larbi Boudad, Abderrahmane El Harradji, Jean-Philippe Degeai, Nicole Limondin-Lozouet

Alluvial records of the African Humid Period from the NW African highlands (Moulouya basin, NE Morocco).

Bruno Depreux [a,b]*, David Lefèvre [a,b], Jean-François Berger [c], Fatima Segaoui [d], Larbi Boudad [d], Abderrahmane El Harradji [e], Jean-Philippe Degeai [a,b], Nicole Limondin-Lozouet [f]

[a] Université Paul Valéry Montpellier 3, CNRS, MCC, UMR 5140 ASM, Montpellier, France

[b] LabEx ARCHIMEDE, Université Paul Valéry Montpellier 3, Campus St Charles, Montpellier, France

[c] CNRS, Université Lumière Lyon 2, UMR 5600 EVS-IRG, Lyon, France

[d] Université Mohammed V, Faculté des Sciences, Rabat, Morroco

[e] Université Mohamed 1[er], Faculté des Lettres et des Sciences Humaines, Oujda, Morocco

[f] CNRS, Université Paris 1 and Université Paris-Est Créteil, UMR 8591 LGP, Meudon, France

* Corresponding author:

E-mail address: bruno.depreux@univ-montp3.fr

Full postal address: Bruno Depreux, Université Paul Valery Montpellier 3, Route de Mende, UMR 5140 – ASM, 34199 Montpellier cedex 05, France

Abstract

This paper presents Early to Late-Holocene sedimentary deposits from the Moulouya catchment, the main Mediterranean river basin of Morocco. Within this region, recent studies have focused particularly on marine or lacustrine archives. Studies on fluvial archives are thus important for improving our understanding of palaeoenvironmental responses to Holocene climatic changes at regional and supra-regional scales. Here, we studied alluvial archives from two basins 300 km apart in the mid-Moulouya basin and High-Plateaus region located in the rarely studied NW African highlands, which are currently defined by arid and cold climatic conditions. Strong similarities between these deposits in terms of morpho-pedosedimentary and chronostratigraphical evolution demonstrate a regional morphogenic pattern controlled by Holocene climatic changes. Using a multi-proxy approach, we document rapid palaeoenvironmental changes and orbital-scale morphogenic changes. Four particular phases of regional geomorphic stability have been dated to ca. 10800–10500, 10200–9900, 9300, and 8900 cal. BP. Enhanced flooding periods that reflect times of climatic aridification may correlate with Early and Mid-Holocene Rapid Climatic Changes, especially during the 9.2 ka event. Furthermore, the Moulouya alluvial archives record the development of an extensive wetland formation and tufa sedimentation within the alluvial plains between ca. 10.8

to 6-5 cal. ka BP. This formation is recognised at a regional scale across the upper and mid-Moulouya catchments, whereas it is missing from other Moroccan fluvial archives. These lasting humid climatic conditions (ca. 10.8–6/5 ka cal. BP.) are consistent with those recorded in the sub-Saharan records during the last African Humid Period (AHP), and suggest a potential linkage between the NW African highlands and the Saharan domain. Hence, we assume that this wetland formation located at 32°–34°N is consistent with the northern archives recording AHP wet conditions.

Keywords: Holocene; Fluvial geomorphology; Palaeoclimatology; North Africa; Morocco; Moulouya basin; Rapid Climatic Changes (RCCs); African Humid Period (AHP); Wetland;

1 Introduction

NW Africa occupies a special place in environmental and climatic studies because the region lies in subtropical latitudes surrounded by the Mediterranean Sea, Atlantic Ocean, and Sahara Desert, and is affected in complex ways by their respective atmospheric regimes. Strong connections of the Western Mediterranean area (Iberian Peninsula and NW Africa) with the North Atlantic realm are evident. At a millennial scale, correlations between Atlantic Bond events and Holocene Rapid Climatic Changes (RCCs) recorded in Western Mediterranean marine studies were documented, notably with cold events revealed by declines of the forest cover and sea surface temperature (SST) cooling (Cacho et al., 2001; Fletcher and Sanchez-Goñi, 2008; Combourieu-Nebout et al., 2009). The so-called “Bond events” correspond to a succession of Holocene ice-rafting events in the subpolar North Atlantic documented by Bond et al. (2001). These events, based on the counting of haematite-stained grains in marine cores, indicate cooling phases related to reductions of the thermohaline circulation in the North Atlantic and beyond. Indeed, hydro-climatic teleconnections between the North Atlantic cooling phases and the Moroccan precipitation anomalies are recognised and demonstrate the key role of the area for reconstructing Holocene climatic and palaeoenvironmental changes (Zielhofer et al., 2019). At an orbital scale, Saharan archives from lower latitudes provide evidence of Early and Mid-Holocene humid climatic conditions lasting over millennia and due to solar-driven summer insolation maxima. This long-term climatic alteration, commonly referred to as the African Humid Period (AHP), resulted in a monsoon regime extending further north than today, and favouring the development of a vegetated landscape dotted with lakes across the currently hyperarid Sahara (Gasse, 2000; Gasse, 2002; Kröpelin et al., 2008; Lézine et al., 2011; Shanahan et al., 2015).

In NW Africa, the sub-humid Moroccan terrestrial archives, i.e. lacustrine and speleothem records ranging from the Atlantic coast to the Middle Atlas range, demonstrate the sensitivity of the westernmost Mediterranean and North Africa to the Atlantic regime (Lamb et al., 1995; Wassenburg et al., 2016; Zielhofer et al., 2017a; Ait Brahim et al., 2019; Zielhofer et al., 2019). Wassenburg et al. (2016) demonstrated that Western Mediterranean rainfall variability on a millennial timescale was positively correlated with rainfall measured in northern Europe during the Early Holocene. Zielhofer et al. (2017a, 2019) revealed an in-phase pattern between Early Holocene winter rain minima and cooling events, and demonstrated the influence of the North Atlantic Oscillation (NAO)-like atmospheric mode in this region during the Mid-to-Late Holocene. Furthermore, Zielhofer et al. (2017b) documented Saharan dust inputs in the Sidi Ali lake reflecting the Mid-Holocene aridification. Other Saharan impacts have been evidenced by a High Atlas speleothem record located on the Atlantic coast, which indicates a strong linkage with the Saharan domain, thereby proposing a new record of the West Africa (WA) monsoon (Sha et al., 2019).

The NW African palaeoenvironmental framework has improved over the last twenty years, mostly because of the inclusion of marine records from the Alboran Sea and Atlantic coast (Cacho et al., 2001; Fletcher and Sanchez-Goñi, 2008; Combourieu-Nebout et al., 2009; McGee et al., 2013; Tierney et al., 2017), and speleothem and lacustrine records from the Middle Atlas Mountains (Lamb et al., 1995; Cheddadi et al., 1998; Rhoujjati et al., 2010; Nour El Bait et al., 2014; Tabel et al., 2016; Wassenburg et al., 2016; Fletcher et al., 2017; Zielhofer et al., 2017a, 2017b; Ait Brahim et al., 2019; Zielhofer et al., 2019). In contrast, fluvial studies in this region are not so numerous or recent, with the region suffering from a paucity of high-resolution alluvial records analysing the responses of the river systems to long- and short-term climatic changes and forcing factors. However, these are of crucial importance for improving our understanding of the palaeoenvironmental conditions of the river catchments and their evolution in response to Holocene climatic changes at regional and supra-regional scales. Moreover, they give an environmental and ecological framework essential to archaeological research. The Medjerda river system in Tunisia is the only one to have been comprehensively studied with a systemic and integrated approach, and it demonstrated Holocene flooding periods coinciding with cold events (Faust et al., 2004; Zielhofer et al., 2004; Zielhofer and Faust, 2008). In Morocco, fluvial studies have focused particularly on the Mediterranean coast, with two of them having described the morphosedimentary evolution of the Kert basin (Barathon et al., 2000; El Amrani et al., 2008), although Zielhofer et al. (2008) described an alluvial formation that was missing from the Holocene fluvial history of this basin. One recent study dealing with a palaeomeander of the main Moulouya stream remains the most detailed description of the Mid- and Late Holocene floodplain deposits (Ibouhouten et al., 2010; Zielhofer, et al., 2010). Studies concerning the upstream sections of the Moulouya basin are even rarer and older. Lefèvre (1985) was the first to lay the foundations for an understanding of the Holocene alluvial formations in the mid-Moulouya basin, then Limondin-Lozouet et al. (2013) developed palaeoecological approaches to characterise the Early and Mid-Holocene environmental conditions. To this day, Wengler's work remains the only study investigating the alluvial archives of the Moroccan High-Plateaus, with the authors compiling several alluvial formations through the Holocene, with notable Early Holocene deposits (Wengler and Vernet, 1992; Wengler et al., 1992; Wengler et al, 1994).

Thus, as studies tend to be concentrated on the Atlantic and Mediterranean coasts, knowledge on the hydrological evolution of the NW African highlands, which are delimited by the Atlas mountain ranges and stretch from Morocco to Tunisia, remains scarce. However, this region, which forms the margins of the Sahara Desert, should be considered a key region, as it is connected to the Mediterranean, Atlantic, and Saharan atmospheric regimes (Knippertz and Wernli, 2010). In this context, this article focuses on alluvial archives from two basins of the NW African highlands, namely the mid-Moulouya and the High-Plateaus areas. Two main alluvial outcrops, which are representative of the Holocene formations at a regional scale, have been chosen and dated with a total of twenty-one radiocarbon dates. Using a multi-proxy approach combining sedimentological, geochemical, and malacological analyses, the aim of this study was to compare and analyse similarities between the alluvial archives of these two basins, to reconstruct the regional hydrosedimentary and morphogenetic patterns during the Early to Mid-Holocene. Comparisons of our results with other NE Moroccan fluvial archives and proxies at different scales from the Mediterranean, Atlantic, and Saharan domains should provide new insights into hydrological evolution of the NW African highlands and the palaeoenvironmental responses to Holocene climatic changes.

2 Regional settings

2.1 The Moulouya catchment

The Moulouya is the largest Mediterranean river basin in Morocco (ca. 65 000 km²). The basin is delimited by the main NW African mountain ranges: the High and Saharan Atlas bordering the Sahara to the south, the Middle Atlas and the Rif blocking the Atlantic air masses to the west, and the Beni Snassen and Oujda mounts from the Tell Atlas ranging along the coast to the northeast (Fig. 1). Hence, the Moulouya basin has the peculiarity of constituting a border area between the Atlantic and Saharan major drainage basins, as it shares a 500+ km length of the Mediterranean-Atlantic watershed to the west, and 600+ km length of the Mediterranean-Saharan watershed to the south and east.

Furthermore, within the Moulouya basin, one may distinguish both the main stream of the Moulouya River flowing from the Atlas ranges to the Mediterranean Sea, and the Za River, its widest tributary, which drains nearly half of the Moulouya basin drainage area (ca. 30 000 km²).

The SW–NE oriented Moulouya River, which flows across successive large basins filled by Neogene and Quaternary sedimentary formations, is heavily influenced by the geological and tectonic patterns of its upper and middle reaches. Its southern side drains the northern slopes of the High Atlas (W–E trend) and its northern side drains the south-eastern slopes of the Middle Atlas (SW–NE trend), with both the High Atlas and Middle Atlas being composed of mainly Lower to Middle Jurassic carbonate rocks. The lower reach of the Moulouya is delimited by the Rif Mountains to the west and the Tell Atlas to the east.

In comparison, the Za River drains the westernmost part of the High Plateaus region, which corresponds to the NW African highlands stretching from Morocco to Tunisia. These highlands encompass the Saharan Atlas to the south, the Tell Atlas to the north, and the Aures range to the east. The High-Plateaus region is defined by 1000–1300 m-high steppe plateaus dotted with several *chotts* (seasonally-dry salt lakes). The Moroccan High Plateaus are mostly composed of Lower to Middle Jurassic series with a few Middle to Upper Cretaceous series in the Rekkam, Debdou-Mekkam, and Trarit mounts (Médioni, 1960; Michard et al., 2008), which are overlaid by flat Neogene lacustrine limestone and Quaternary conglomerates in the northern part (Stretta, 1952).

Whereas the lower Moulouya displays a semi-arid Mediterranean climate with a rainfall regime predominantly driven by winter precipitation, the upper Moulouya catchment is characterized by a spring rainfall maxima (Thornes et al., 2009; Sebbar, 2013). The middle and upper reaches of the Moulouya and the High Plateaus are defined by arid and cold climatic conditions classified as “cold desert climate” (BWk) in the Köppen-Geiger system (Beck et al., 2018). Orographic conditions are a controlling factor, with the Moulouya basin lying in the rain shadow of the Middle Atlas, which mitigates the rainfall from the Atlantic westerlies and produces dry air masses. The upper Moulouya Basin is characterized by low precipitation (150–200 mm/year), which falls mostly in the spring time, although the highest summits of the mountain areas form an exception to this, with more intense rainfall (e.g. around Debdou, El Harradji 1985, 2019). The high interannual temperature together with the high rainfall amplitudes (Sebbar, 2013) lead to a steppe like vegetation composed mainly of Esparto (Stipa tenacissima) and Chih (Artemisia herba alba).

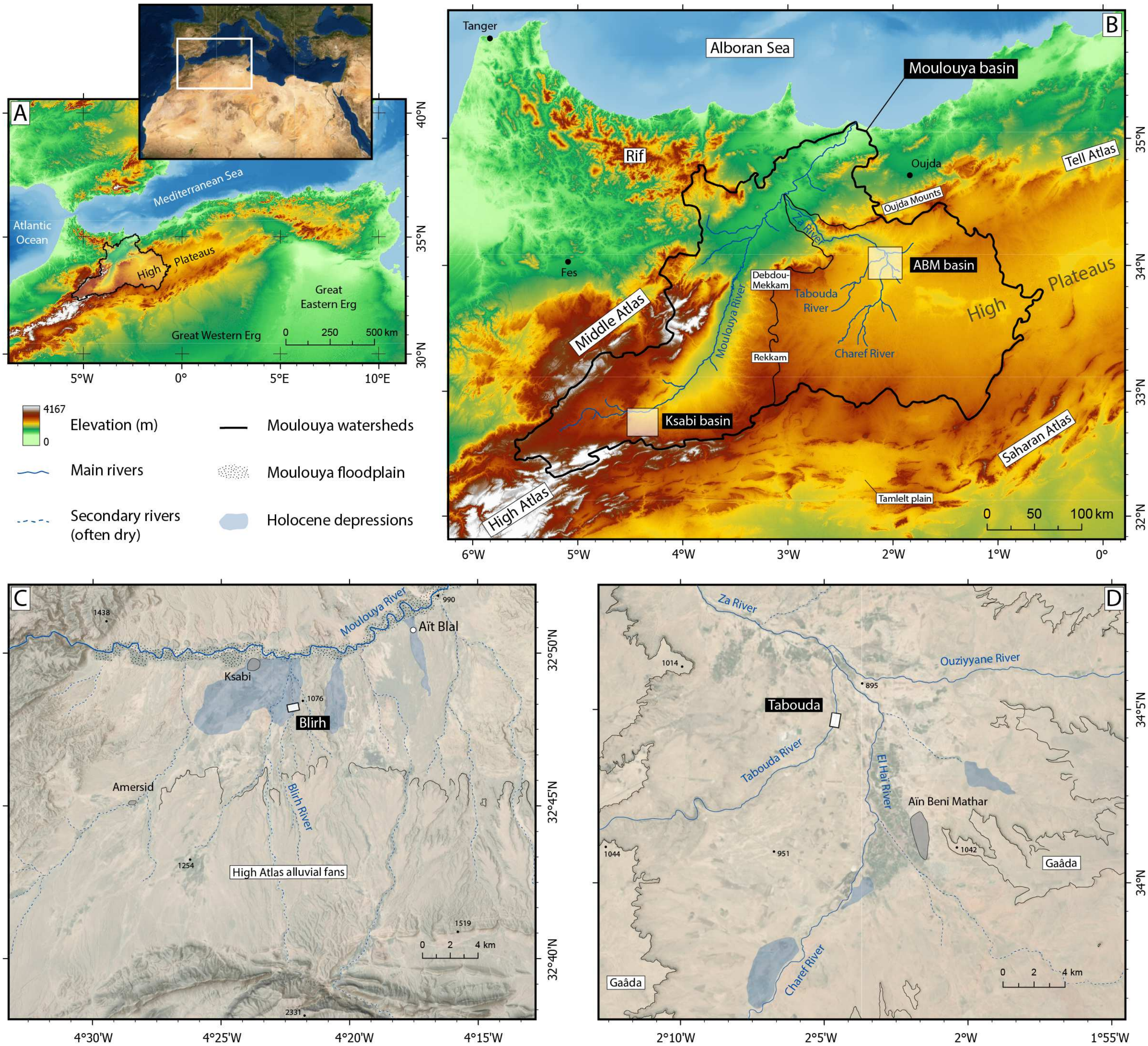

Fig. 1. Geographical settings. A) Satellite image of North Africa with the NW Africa digital elevation model (DEM) and the location of the Moulouya catchment. B) Map of the Moulouya catchment with localisation of the Ksabi basin in the middle reach of the Moulouya, the Aïn Beni Mathar basin (ABM basin) in the northern High Plateaus region, and the main geophysical features discussed in the paper. C) Satellite image with hill-shade elevation of the Ksabi basin and localisation of the Blirh river section. D) Satellite image with hill-shade elevation of the ABM basin and localisation of the Tabouda river section. The DEM and satellite images were obtained from ASTER (NASA et al., 2009) and TerraColor imagery respectively (Esri, 2009).

In these continental highlands, the current hydrographic systems are characterised by entrenched river streams and nested terrace systems. Headward erosion strongly affects the bare riverbanks resulting in the formation of badlands, thereby representing an important sediment yield. The flow regime is intermittent: dry for part of the year, but with the rivers marked by high-energy short-term flows when heavy rainfall occurs. Such arid catchments are particularly fragile and sensitive to climatic changes (Fletcher and Zielhofer, 2013), with aridity and (flash) floods having serious impacts on these hydro-ecosystems, with the formation of a negative feedback loop that produces reduced soil moisture and vegetation cover, and higher runoff and sediment erosion, which have worsened further as overgrazing has increased in the course of the 20th century (El Harradji, 1997).

2.2 Study areas

This study focuses on two basins in these continental highlands, the Ksabi basin and the Aïn Beni Mathar (ABM) basin (Fig. 1B). These basins are located 300 km apart from each other, which allows local and regional factors controlling the geomorphological and palaeoenvironmental evolution of the arid river catchments to be differentiated. The Ksabi basin is a Neogene sedimentary basin located in the upper middle course of the Moulouya River. The Moulouya River exhibits a stepped terrace system incised into Neogene gypsiferous red claystone. This system consists of a complex of at least seven Pleistocene coarse alluvial formations that are generally protected by calcrete, stretching from the maximum incision of the present-day valley to a height of 150 m above it (Lefèvre, 1985; Lefèvre, 1989). The ABM basin in the northern High-Plateaus is a Cenozoic basin filling a paleo-depression resulting from normal faults that deformed the Jurassic bedrock and led to a horst-graben formation (El Harradji, 1985, 1994; Bouazza et al., 2013; El Harradji, 2019). The lacustrine limestone and dolostone have eroded as an endorheic system since the Pleistocene, forming *gaâda* (i.e., tabular and stony conglomerate escarpments around the basin; Fig. 1c, Stretta, 1952).

To understand the spatio-temporal variability of Holocene sedimentary formations at a local scale, fieldwork was conducted on several river sections within these basins. The field surveys revealed extended Early to Mid-Holocene fluvio-palustrine deposits in the ABM and Blirh floodplains. These deposits, which are recognisable by their dark-grey and flat facies, constitute an extensive formation in every tributary river investigated. In the Ksabi basin, the Blirh River is a small tributary on the southern side of the Moulouya River, which originates from the alluvial fans of the northern High Atlas piedmont (Fig. 1C). Previous studies have already documented the Holocene sedimentary and palaeoecological evolution of its floodplain: Lefèvre (1985, 1989) attributed the fluvio-palustrine deposits to the Early Holocene and documented them within the Blirh and Aït Blal outcrops (Fig. 1). Thereafter, later studies developed palaeoecological approaches to characterise the Early and Mid-Holocene environmental conditions (Lefèvre and Ballouche, 1991; Limondin-Lozouet et al., 2013). In the ABM basin, the Tabouda River, one of the most important tributaries of the Za River, showed large outcrops of these dark-grey and flat deposits (Fig. 1D). In this paper, one alluvial outcrop representative of the Holocene fluvio-palustrine formations will be presented for each basin, and will be subjected to multi-proxy analyses.

3 Material and Methods

The hydrosedimentary dynamics of both study areas were investigated using a multi-proxy approach combining sedimentological, geochemical, and palaeoecological analyses.

3.1 Lithostratigraphy and sampling

The current river beds, which are deeply entrenched within their floodplains, facilitate observation and access to river bank outcrops (Fig. 2, Fig. 3). The choice of the studied alluvial outcrops mostly depended on the maximum thickness, diversity, and preservation of the pedosedimentary formations. The descriptions of these alluvial deposits are realised in terms of their architecture and pedosedimentary facies, which reveal discontinuities or erosional layers within the formation. Then, sedimentary units were defined and grouped into sedimentary sequences which indicate depositional environments. Each outcrop was sampled every 3–5 cm, depending on the pedosedimentary facies. A total of 272 samples were collected for the multi-proxy analyses: 131 samples from the 3.55-m high Tab01 outcrop and 141 samples from the 5.70-m high Bli01 outcrop. Previous studies at Blirh resulted in fieldwork, radiocarbon dating, and sedimentological and geochemical analyses on the same profiles and cross-sections, to facilitate comparisons with malacological data (Limondin-Lozouet et al., 2013).

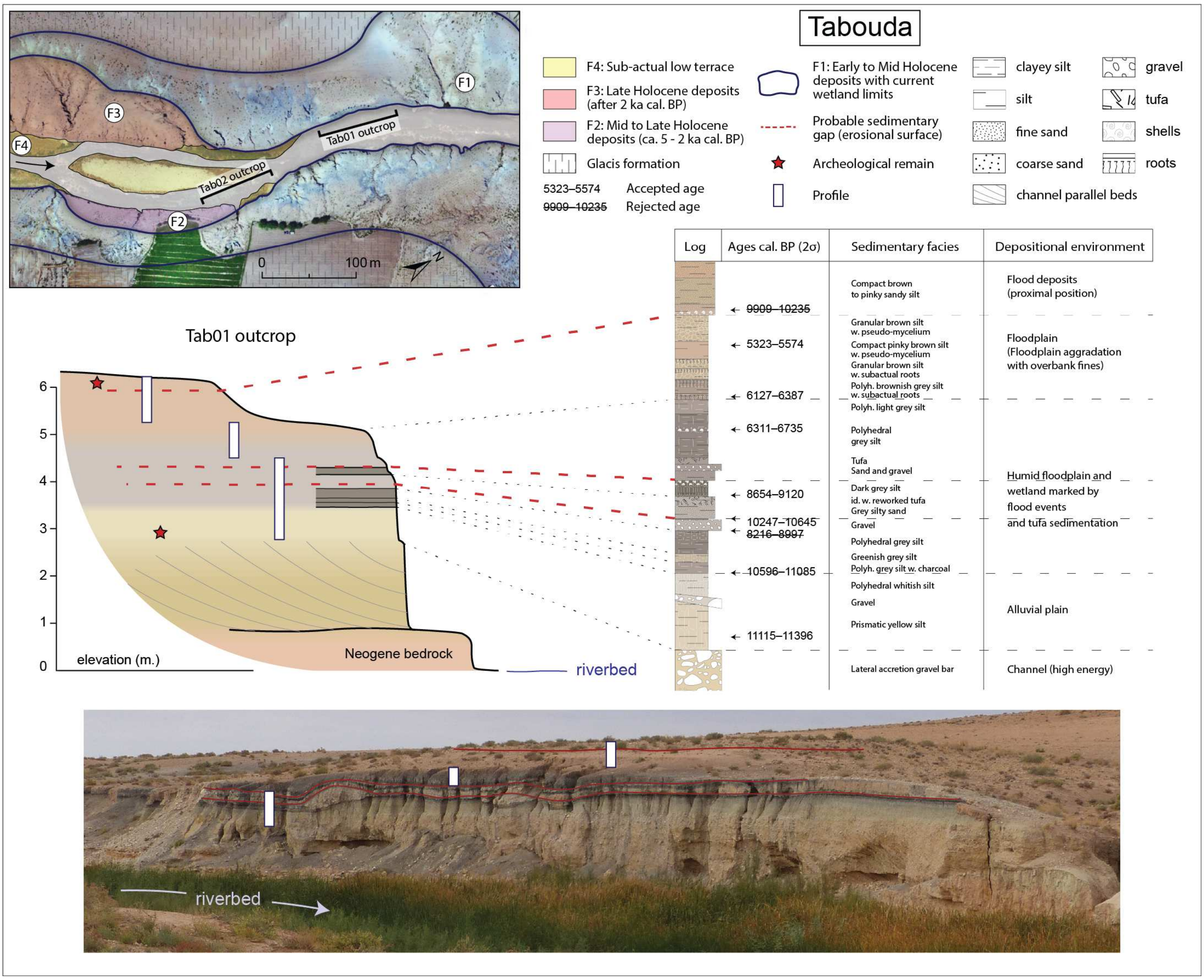

Fig. 2. Geomorphological and sedimentological settings of the Tabouda formation, including a synthetic geomorphological map of the Tabouda river section with localisation of the Holocene cut-and-fill and nested alluvial formations (F1 to F4). F1 indicates the Early to Mid-Holocene unaltered wetland formation revealed by headward erosion. Tab01 outcrop: synthetic cross-section with corresponding sedimentological features and calibrated radiocarbon dates, and photograph of the outcrop.

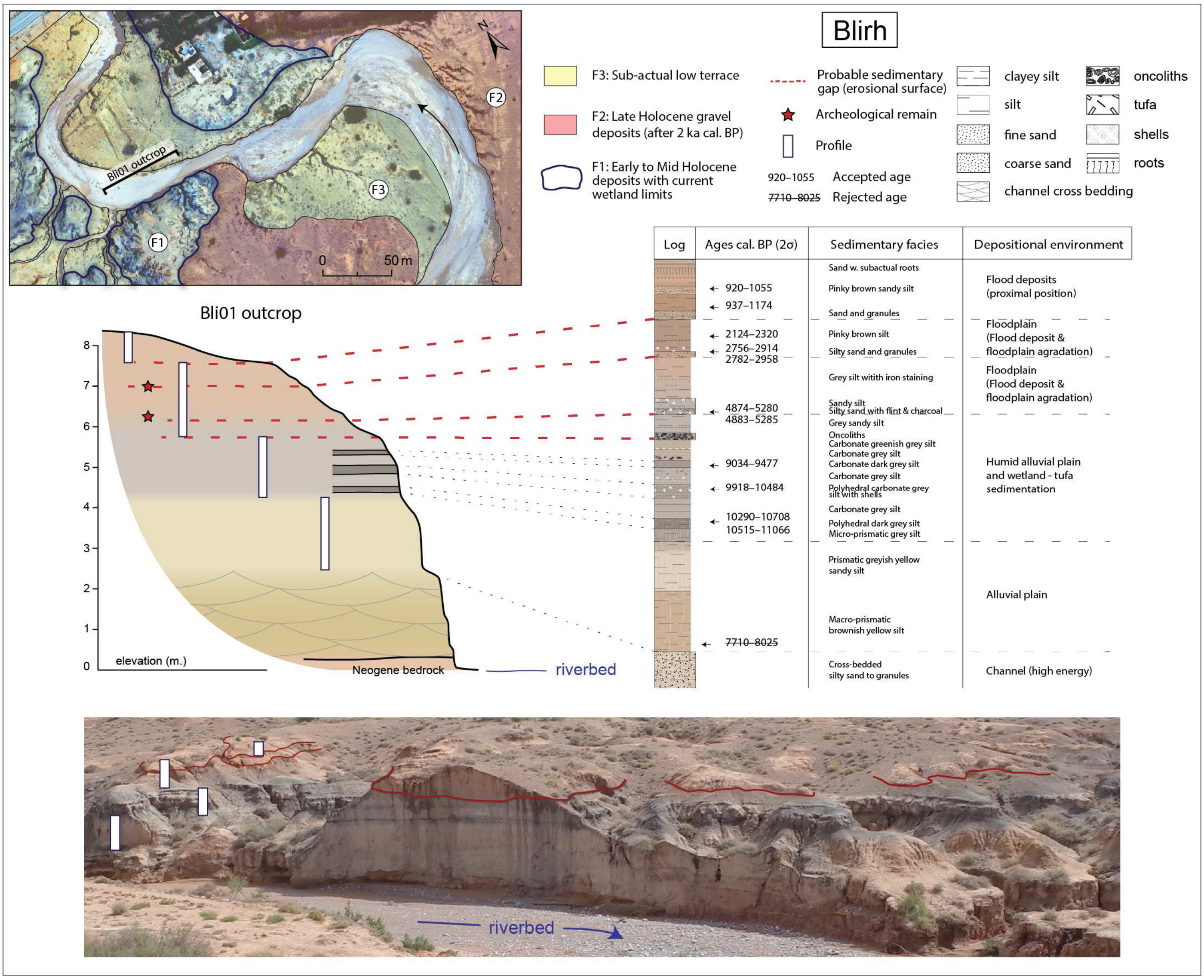

Fig. 3. Geomorphological and sedimentological settings of the Blirh formation, including a synthetic geomorphological map of the Blirh river section with localisation of the Holocene cut-and-fill and nested alluvial formations (F1 to F3). F1 indicates the Early to Mid-Holocene unaltered wetland formation revealed by headward erosion. Bli01 outcrop: synthetic cross-section with corresponding sedimentological features and calibrated radiocarbon dates, and photograph of the outcrop.

3.2 Chronology

Twenty-one AMS radiocarbon datings have been performed on the two sedimentary outcrops: 16 new dates on charcoal materials and 5 dates on organic bulk sediment previously published by Limondin-Lozouet et al. (2013). These dates are in good accord, despite the difference in material (Table 1). All these radiocarbon-derived ages were calibrated using IntCal20 (Reimer et al., 2020). Three of them were rejected: Bli01 C2 17 sample because bulk was dated in the absence of charcoal with low amount of likely inorganic carbon (0.08 mg), Tab01 no. 7 sample which was not pure charcoal with very low amount of measured carbon (0.03 mg), and Tab01 no. 16 sample that could be an old charcoal transported by a flood. Six other AMS radiocarbon datings have been performed on other river sections or outcrops.

Table 1. Chronological data for the Tabouda and Blirh alluvial deposits: conventional radiocarbon ages and calibrated ages (* taken from Limondin-Lozouet et al. 2013).

Section/Outcrop	ID code	Lab no.	Depth (cm)	Material	Age ^{14}C BP	Age cal. BP (2-σ)	Age cal. BP (median)
Tabouda (Tab01)	TAB01 no. 16	Poz-89112	46	charcoal	8970 ± 50	9909–10235	10128
Tabouda (Tab01)	TAB01 no. 14	Lyon-14542	75	charcoal	4710 ± 30	5323–5574	5400
Tabouda (Tab01)	TAB01 no. 13	Poz-110518	126	charcoal	5460 ± 40	6127–6387	6249
Tabouda (Tab01)	TAB01 no. 12	Poz-110517	154	charcoal	5730 ± 100	6311–6735	6529
Tabouda (Tab01)	TAB01 no. 9	Poz-89176	213	charcoal	8050 ± 50	8654–9120	8910
Tabouda (Tab01)	TAB01 no. 8	Poz-116777	236	charcoal	9260 ± 70	10247–10645	10431
Tabouda (Tab01)	TAB01 no. 7	Poz-110516	247	charcoal	7750 ± 150	8216–8997	8571
Tabouda (Tab01)	TAB01 no. 1	Poz-89110	285	charcoal	9520 ± 50	10596–11085	10851
Tabouda (Tab01)	TAB01 no. 3a	Poz-89111	343	charcoal	9820 ± 60	11115–11396	11235
Tabouda (Tab02)	TAB02 ch.7	Lyon-14543		charcoal	4280 ± 30	4733–4955	4849
Tabouda	TAB S3 no. 15b	Lyon-15933		charcoal	10015 ± 45	11281–11737	11507
Blirh (Bli01)	BLI01 C5 55-56	Lyon-16051	45	charcoal	1060 ± 30	920–1055	958
Blirh (Bli01)	BLI01 C5 80	Lyon-16052	70	charcoal	1115 ± 30	937–1174	1013
Blirh (Bli01)	BLI01 C4 50	Poz-116779	113	charcoal	2205 ± 30	2124–2320	2231
Blirh (Bli01)	Blirh 08 f 1B*	Poz-40744	134	charcoal	2725 ± 35	2756–2914	2817
Blirh (Bli01)	Blirh 08 f 1A*	Poz-40743	134	charcoal	2780 ± 35	2782–2958	2876
Blirh (Bli01)	Blirh 08-02 20B*	Poz-40750	220	charcoal	4435 ± 35	4874–5280	5038
Blirh (Bli01)	Blirh 08-02 20A*	Poz-40749	220	charcoal	4450 ± 35	4883–5285	5110
Blirh (Bli01)	Blirh 08-01 4*	Poz-40747	300	organic sediment	8310 ± 70	9034–9477	9312
Blirh (Bli01)	Blirh 08-01 3*	Poz-40746	334	organic sediment	9060 ± 70	9918–10484	10223
Blirh (Bli01)	Blirh 08-01 2A*	Poz-40799	382	organic sediment	9330 ± 70	10290–10708	10531
Blirh (Bli01)	Blirh 08-01 2B*	Poz-40745	382	organic sediment	9450 ± 50	10515–11066	10686
Blirh (Bli01)	BLI01 C2 17	Poz-116780	560	bulk	7080 ± 80	7710–8025	7895
Blirh (C12)	C12 ech.16	Poz-77059		charcoal	9400 ± 50	10445–10757	10628
Aït Blal	AB 39	Poz-102688		charcoal	8650 ± 160	9320–10184	9704
Charef (Cha01)	CHA01 no. 1	Poz-89054		charcoal	8840 ± 50	9700–10157	9927
Si Bou Ramdane	C13b ech.22	Poz-77094		charcoal	9000 ± 70	9897–10276	10151

3.3 Sedimentological analyses

3.3.1 Mass-specific magnetic susceptibility

Mass-specific magnetic susceptibility (MS) was measured with a Bartington MS2B dual frequency sensor. The measurements were undertaken on dried and powered homogenised samples at an operating frequency of 4.65 kHz using a range of 0.1 with a period of 15 s (1 x 10^{-8} $m^3.kg^{-1}$). Diamagnetic materials such as organic matter, quartz, and calcite give very low negative values, and in our case indicate calcareous formations, whereas ferrimagnetic minerals such as iron oxides display high values and indicate soil formation, eroded soil in a secondary position, or provenance changes (Dearing, 1999).

3.3.2 Grain size

Laser grain-size analyses were performed using a Malvern Mastersizer 2000 analyser. Samples were treated with hydrogen peroxide and hydrogen chloride to remove organic matter and carbonate contents, and were then rinsed twice with distilled water after 10 min of stirring. Samples were then treated with a sequence of potassium chloride (7.45 g/L), distilled water, and sodium hexametaphosphate (5.5 g/L) for 4 h before measurement. Several indices were calculated from the raw data to evaluate the flow energy of the rivers, including the clay-silt-sand fractions using 2 µm and 63.5 µm as internal constraints, and the D50, D90, and D99 values, which correspond to the median and coarser sediment percentiles. The median assesses the mean energy of a river flow, and the D99 percentile assesses its maximal energy.

3.3.3 Loss-on-ignition

The loss-on-ignition (LOI) method was used to determine organic matter (OM), silicates/oxides, and carbonate contents (% of the bulk mass). Samples were dried for 12–24 h at 106°C. The OM content was combusted at 550°C over 5 h and the calcium carbonate content was obtained after combustion at 950°C over 2 h (Heiri et al., 2001).

3.3.4 ED-XRF geochemistry and statistical treatment

The chemical composition of the pedosedimentary facies was analysed using energy-dispersive X-ray fluorescence (ED-XRF) spectrometry with a Delta InnovX portable spectrometer. XRF analyses were performed on dried and powered homogenised samples to minimize perturbation effects from factors such as grain-size, porosity, and water content (Zolitschka et al., 2014; Profe et al., 2016). Major and trace elements were measured using a two-beam mining analytical mode (Si, K) and a three-beam soil analytical mode (Ca, Ti, Mn, Fe, Zn, Rb, Sr, Zr). The parameters of the analytical modes included: 10 kV, 0.03 mA, and 5 s (counting time) for the first beam of the mining mode; 40 kV, 0.01 mA, and 10 s for the second beam of the mining mode; 40 kV, 0.07 mA, and 30 s for the first beam of the soil mode; 40 kV, 0.04 mA, and 30 s for the second beam of the soil mode; and 10 kV, 0.045 mA, and 45 s for the third beam of the soil mode. Instrument errors were lower than ± 2% for K, Ca, Fe, and Sr, lower than ± 5% for Mn, Rb, and Zr, and ranged from ± 5 to ± 15% for Si, Ti, and Zn. Elements lighter than Si were not measured given the counting times.

Multivariate statistical analyses were conducted to interpret and compare the major and trace element contents of both sedimentary formations. These geochemical data are expressed as relative concentrations (i.e. ppm) and must be considered as compositional data (Aitchison, 1982), and are therefore subject to spurious correlations that may infer statistical biases if classical multivariate analyses are used. Aitchison (1986) provided a reliable solution by transforming the raw percentages to log-ratios. Prior to principal component analyses (PCA), all the geochemical data were centred log-ratio (CLR) transformed (Comas-Cufí and Thió-Henestrosa, 2011) using CoDaPack software. Then, a PCA based on the covariance matrix were conducted for each sedimentary formation. The first three principal components (PCs) extracted were plotted against depth, with indication of their variance and the correlations between the variables and factors. These correlations, usually plotted in a correlation circle, are useful for interpreting the meaning of the axes, i.e., indicating which elements are responsible for each axis factor. These data are specified in Tables 2 and 3, which also present squared cosine (cos^2) values that estimate the quality of the representation of each variable: the greater the cos^2, the greater the link with the corresponding axis.

3.4 Malacology

Malacological data from Limondin-Lozouet et al. (2013) were exploited, and new data obtained from the Tabouda deposits are presented in this paper. For the Tabouda outcrop, 19 2-kg samples of sediment were collected for each sedimentary unit, whereas for the Blirh outcrop, 41 8-kg samples were collected at 10-cm intervals. The samples were wet sieved through 0.5-mm mesh, dried, and complete and broken shells were sorted under a binocular microscope. The numbers of each species were counted according to the established rules for counting shells, and detailed malacological analyses were based on the determination and classification of the species into ecological groups according to factors controlling their abundance and distribution, such as humidity, temperature, plant formations, altitude, and geographical zonation (Puisségur, 1976).

4 Results

4.1 Tabouda River

4.1.1 Chronostratigraphy and morphodynamic evolution

Several alluvial deposits of different ages have been identified along the riverbanks of the Tabouda river and result from a cut-and-fill fluvial system. Surveys performed in the basin showed that the oldest Holocene formation (Fig. 2), which is recognisable by its dark, fine, and flat deposits, can be identified at different localities (Fig. 8).

This formation extends across the width of the alluvial plain and is well represented at a regional scale. Following on from this formation, several incision-aggradation phases led to alluvial deposits during the Mid- and Late Holocene, such as the one at Tabouda (Tab02 outcrop) starting from ca. 5000 cal. BP (Fig. 2, F2 to F4, Fig. 8). In this study, we focus on the oldest formation, and specifically on an exposure located on the western bank of the Tabouda River (Tab01 outcrop). These deposits are composed of 26 lithopedosedimentary facies grouped into 11 main sedimentary units and 6 sedimentary sequences spanning from 11350 to 4450 cal. BP, although there are probable sedimentary gaps at the Early to Mid-Holocene transition (Fig. 4). The chronology is based on nine radiocarbon dates obtained from charcoal (Table 1).

The first sedimentary sequence at the bottom of the outcrop is a 1.5-m thick pebble deposit that has not been dated. This coarse lateral accretion bar formation is recognisable alongside the exposure for a length of over 30 m, and corresponds to an active meandering channel deposit (Fig. 2). Because of its stratigraphic position and the following Early Holocene sedimentation, this high-energy river deposit can potentially be attributed to the Younger Dryas (YD) cold event (Fig. 2). Following this lateral accretion deposit, fine sedimentation starts with the Early Holocene. Indeed, the onset of this new sedimentary sequence (S1) was dated to 11115–11396 (11235) cal. BP near to the active channel (Fig. 4). However, on the eastern bank further from the channel, another 1-m thick profile of the same sedimentary facies (unit I) and stratigraphic position revealed an archaeological hearth dated at 11281–

11737 (11507) cal. BP. This sedimentary sequence is characterised by macro- to micro-prismatic structure and variegated staining indicating variations in groundwater level.

A clear change in the sedimentation is then evident, with the deposition of a dark organic sedimentary unit characterised by a polyhedral to prismatic structure and thin beds of carbonised plant residues (S2 and unit II). This unit is particularly wide in this profile, becoming thinner laterally along the outcrop; thus, three facies may be distinguished, including a micro-polyhedral greenish silt (IIb). The onset of this sequence was dated to 10596–11085 (10851) cal. BP. The following unit III is composed of gravel, indicating a flood deposit, but can be recognised for only a few meters alongside the exposure where the gravel filled lateral depressions, and is otherwise absent. Thus, we assume the gravel may indicate a crevasse splay deposit, with the rest of the outcrop not showing any erosional discordance. Above this gravel deposit lays a 1-cm thick dark grey silty unit (unit IV) dated to 10247–10645 (10431) cal. BP. The following sandy unit (V), which can be recognised alongside the outcrop, presents a sharp erosional surface at its bottom, which may explain the thinness of the previous unit IV and indicate a clear flood deposit. The end of the unit (IVb) is marked by the presence of reworked shells and tufa tubes. This deposit marks a new sedimentary sequence (S3) that is covered by a dark and micro-prismatic silty unit (VI) dating to 8654–9120 (8910) cal. BP, which shows a slight mass-specific magnetic susceptibility (MS) increase.

The next sequence (S4) starts with coarser deposits (unit VII) composed of a 10-cm thick sand deposit covered by a gravel deposit and finally reworked tufa tubes, which indicate another flood period. This deposit is covered by a grey polyhedral silty sediment (units VIII and IX) presenting a level containing shells dated to 6311–6735 (6529) cal. BP, and ending at ca. 6200 (6127–6387) cal. BP. This sequence is followed by a change towards brownish coloured silts coinciding with the beginning of an increase in MS values (units X and XI), which seem to correspond with a transition in the hydrosedimentary evolution of the river. These silts, dated to 5323–5574 (5400) cal. BP, show sedimentological changes marked by the presence of pedogenic features in some units (XIa and XIc), i.e., a granular structure and pseudo-mycelium, and their high MS values could indicate a trend towards a more terrestrial environment and/or more intense soil erosion dynamics in the catchment. Finally, the last unit (XII), which is undated, is characterised by a sandy deposit that could indicate enhanced and more energetic fluvial activity.

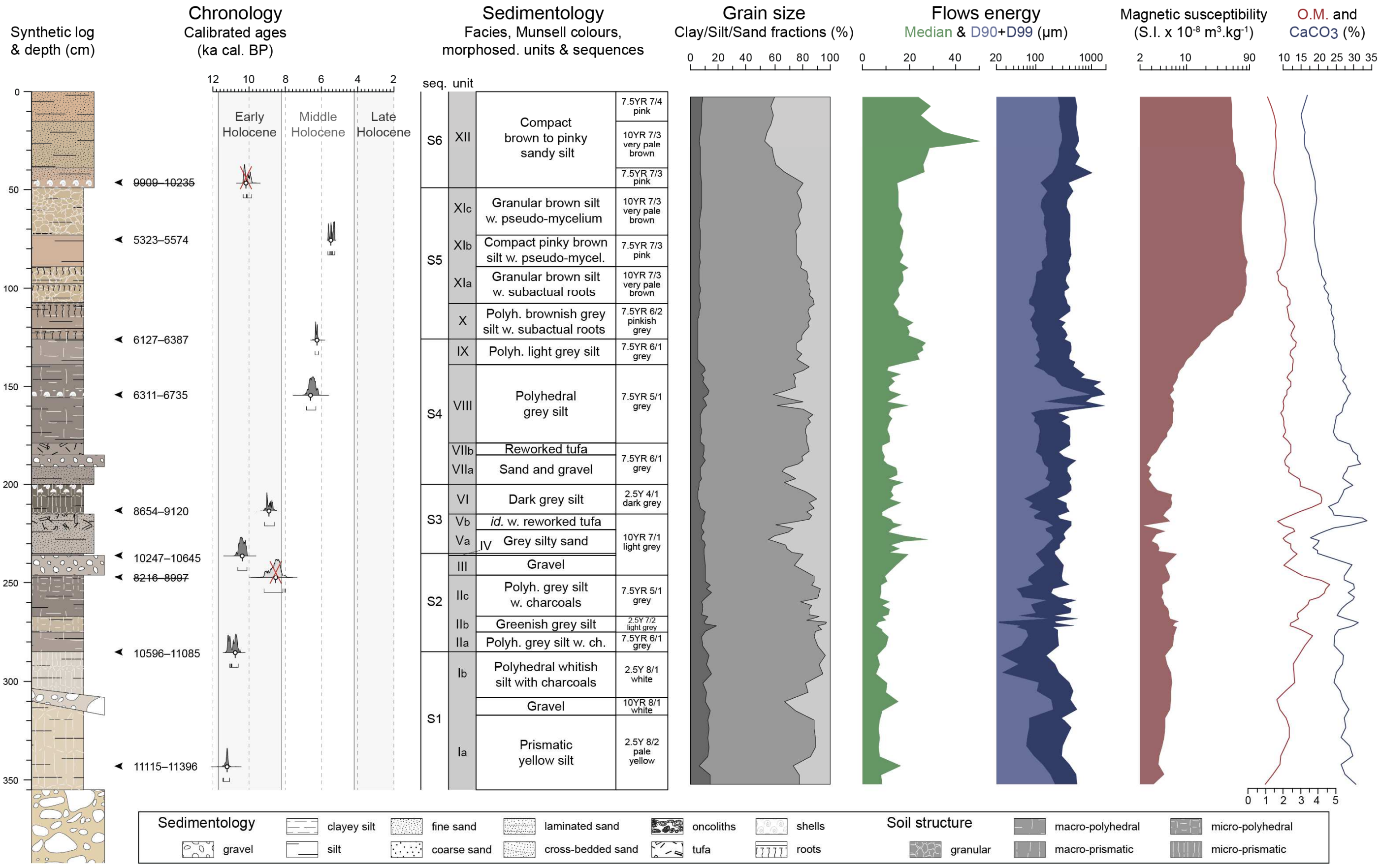

Fig. 4. Analyses of the Tabouda formation – Tab01 – with chronological features, including calibrated ages, a Holocene subdivision timeframe (after Walker et al., 2018), and sedimentological features including descriptions of facies and sedimentary units, grain-size from clay to sand fractions, median and coarse (90 and 99 percentiles) grain-size indices, mass-specific magnetic susceptibility, and organic matter (O.M.) and carbonate contents.

4.1.2 Palaeoecology

The Tab01 outcrop is divided into three mollusc zones (TAB01-MZ 1–3, Fig. 5). MZ 1 is dominated by aquatic species (mainly *Melanopsis* cf. *praemorsa*, *Mercuria similis*, and *Ancylus fluviatilis*), and to a lesser extent, hygrophilous snails, indicating a rather permanent waterbody. Faunal assemblages from TAB01 unit I show a high percentage of aquatic shells (70%), thereby confirming a waterlogged environment. From 10800 cal. BP onwards, aquatic species increased, reaching around 90%–95% of the total assemblage (IIa-b). Then, the proportion of aquatic molluscs decreased, but still prevailed (ca. 70%), with hygrophilous species forming 30% of the assemblage. The strong representation of aquatic species in unit V is consistent with sedimentological features indicating a flood deposit. The dark prismatic sediments (TAB01 unit VI) recorded the highest percentages (almost 50%) of hygrophilous molluscs, whereas the proportion of aquatics species increased again in unit VII. After unit VIII, the MZ 2 phase is characterised by the dominance of hygrophilous species (45%–55%, represented by *Vallonia enniensis*, *Vallonia* *pulchella*, *Carychium minimum,* and *Vertigo antivertigo*), a decreasing proportion of aquatic species (25%), and the appearance of xerophilous species (15%–20%). This progressive change demonstrates drying but still partly humid riverbanks under the development of terrestrial habitats, which is in accordance with the hydrosedimentary transition observed in the sedimentological data. There is then a shift in the shell assemblages at 6200 cal. BP, with aquatic species almost disappearing (5%), and both xerophilous and hygrophilous species present in high percentages (ca. 40%–50% each), indicating a clear drying up of the riverbanks and probably a more intermittent regime of the river (TAB01-MZ3). This trend is confirmed by a maximum of xerophilous shells (75%, mainly composed of *Truncatellina cylindrica* and *Cernuella virgata*) in unit XIb, after which the proportion of xerophilous species stabilises at around 50% and aquatic species increase to around 30%, consistent with the sedimentological data.

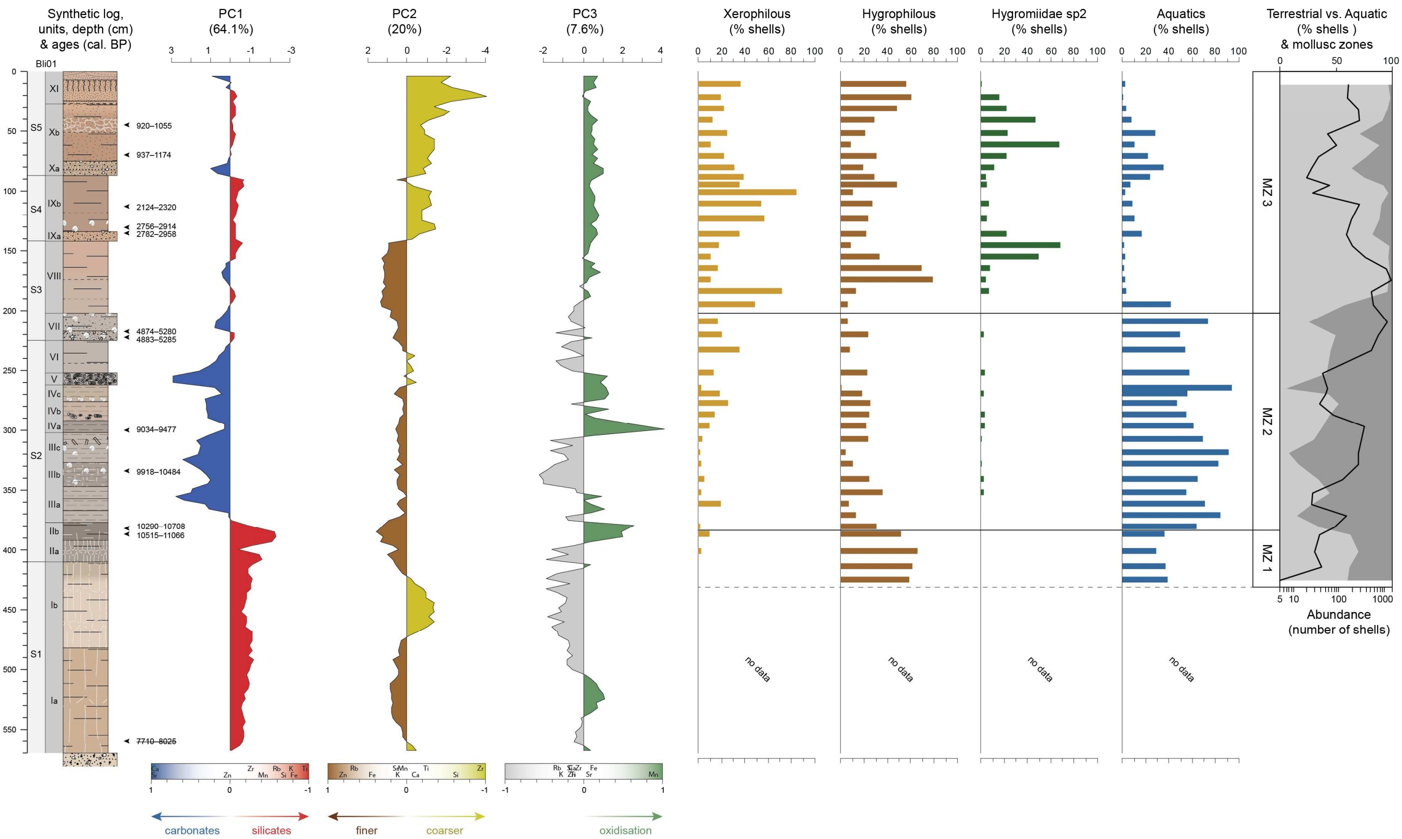

Fig. 5. Analyses of the Tabouda formation – Tab01 – with the statistical results from the ED-XRF analyses, including the first three principal components and their correlations with the variables and their interpretations, and the malacological results (i.e. hygrophilous, xerophilous, aquatic shell contents, and terrestrial [hygrophilous + xerophilous] vs aquatic species percentages with the abundance of shell and mollusc zones).

4.1.3 Geochemical proxies

4.1.3.1 Statistical features

PCA was used to analyse the correlations between the major and trace elements and to give a statistical interpretation of the chemical composition of the pedosedimentary units. The first three PCs represented 88.5% of the total variance of the data. The highest $\cos^2$ value of each element was associated with these first three components, helping to verify the quality of the data representations obtained (Table 2). The following palaeoenvironmental interpretations and geochemical trends extracted from the axis factors were found to be supported by an Agglomerative Hierarchical Clustering (AHC) analysis, which revealed several clusters of elements: Ca-Sr, Zr-Ti-Si-K, Zn-Fe-Mn, and Rb (Fig. S1).

Table 2. Principal components analysis of the Tabouda outcrop. Highest values are marked in bold.

	PC1	PC2	PC3
Variance (%)	50.66	27.34	10.53
Cumulative variance (%)	50.66	78.00	88.53
Factor/Variable correlations			
Si	**0.583**	0.526	−0.106
K	**0.679**	0.233	−0.118
Ca	**−0.953**	0.240	0.049
Ti	**0.652**	0.502	−0.259
Mn	0.353	−0.296	**0.876**
Fe	0.251	**−0.701**	0.101
Zn	**0.731**	−0.606	0.010
Rb	0.271	−0.276	**−0.543**
Sr	**−0.893**	−0.380	−0.184
Zr	0.065	**0.917**	−0.198
$\cos^2$ values			
Si	**0.340**	0.277	0.011
K	**0.462**	0.054	0.014
Ca	**0.908**	0.058	0.002
Ti	**0.425**	0.252	0.067
Mn	0.125	0.088	**0.767**
Fe	0.063	**0.492**	0.010
Zn	**0.535**	0.367	0.000
Rb	0.074	0.076	**0.295**
Sr	**0.798**	0.144	0.034
Zr	0.004	**0.841**	0.039

4.1.3.2 Interpretation of the principal components

The first component represented 50.7% of the variability in the data and showed significant negative correlations with Ca and Sr, and positive correlations with Zn, K, Ti, and Si. Mn, Rb, Fe, and Zr did not show strong correlations with this component (Fig. 5). The negative scores corresponded to carbonate-rich samples, and revealed preserved alluvial deposits such as tufa or coarse fluvial units. Indeed, the Tabouda catchment is almost entirely composed of Middle Jurassic (Bathonian-Bajocian stages) and Lower Jurassic (Sinemurian-Pliensbachuan stages) limestone, which is partly topped by Quaternary desert pavements, except for a small confined area of the Mekkam inlier that consists of schist, quartzite, and basalt rocks. Ca concentrations reached an average of 26% of the total composition of the sedimentary formation and strongly reflect the composition of the underlying bedrock, as it is known that when Ca carbonates are important constituents of sedimentary rocks, most of the Ca is supplied dissolved in stream water (McLennan and Murray, 1999). Therefore, the high Ca content indicates unaltered fluvial deposits coming from the upstream calcareous catchment, but may also indicate tufa deposits formed by precipitation of carbonate minerals (calcite and aragonite), and which existed along the rivers of the ABM basin as waterfalls or tufa barriers (Wengler et al., 1994; El Harradji, 2019). Furthermore, the highest values are correlated with the peaks in the aquatic shell assemblages, which rather supports the secondary precipitation of Ca in solution under palustrine conditions. Positive scores reflect a high amount of siliciclastic content relative to carbonates, and in this floodplain context, they may indicate enhanced weathering processes opposed to Ca and Sr elements. The association of Ca and Sr is indicative of the provenance of calcareous rocks, and because of the high solubility of Ca^{2+} and Sr^{2+} cations in the soil environment, both elements are easily mobilised during weathering (Kabata-Pendias 2001). However, the high content of Zn, K, Ti, and Si may also be derived from other sedimentary sources, or from long-term changes in the drainage system.

The second principal component (PC2) represented 27.3% of the total variance and correlated with Zr and Fe. Positive scores indicated high amounts of Zr, and to a lesser degree, Si and Ti, which reflect increases in coarse-grained fractions interpreted as high energetic fluvial deposits. Indeed, the Zr/Rb ratio is used as a grain-size proxy to trace flooding episodes in an alluvial context (Wang et al., 2011; Jones et al., 2012; Rothwell and Croudace, 2015). Zr is mainly present in the form of the zircon mineral ($ZrSiO_4$), which is highly resistant to weathering and considered to be inherited from the parent rocks (Kabata-Pendias, 2001). For both the Blirh and Tabouda formations, reliable strong correlations were found between the PC2 scores and fine sand content (R_s = −0.808 and 0.790, respectively, with p-value < 0.001). Therefore, the PC2 positive scores at Tabouda seem to mainly reveal coarser sediments deposited in high-energy fluvial environments such as flood events. These findings concern units III-V, VII, and XII at depths of 220–245, 180–200, and 0–40 cm, respectively, and may indicate stronger flooding dynamics related to higher aridity.

Negative scores indicate high Fe and Zn contents, and are interpreted as fine-grained sedimentation, potentially associated with oxidation processes, as opposed to coarse-grained flood events. Indeed, Fe is a major element present in soil, notably as Fe^{2+} in ferromagnesian silicates and as Fe^{3+} in iron oxides and hydroxides resulting from weathering. Dissolved Fe is generally precipitated rapidly with increasing pH-Eh conditions (Kabata-Pendias, 2001). The Zn content of soil depends on the composition of the parent rocks, texture, organic matter, and pH (Mihaljevic, 1999), and its mobility is greatest under oxidising conditions. Given that it is readily adsorbed by mineral and organic soil components (Kabata-Pendias, 2001), notably ferric oxides (Robinson, 1981), Zn usually accumulates in the surface horizons.

The third principal component (PC3) still represented 10.5% of the cumulative variance and mostly represented Mn. Positive scores revealing high Mn content are interpreted as enhanced oxidising conditions, because Mn is highly redox-sensitive (Rothwell and Croudace, 2015). Mn in soil is also strongly dependent on pH-Eh conditions, although other factors can be involved (Kabata-Pendias, 2001), and it exists in three oxidation states (2+, 3+ and 4+) in solids, but only the 2+ state when dissolved in water (Petrie, 1999). Although Mn^{2+} is readily soluble, manganese precipitates in soil under oxidising conditions, because Mn^{3+} and Mn^{4+} cations form insoluble hydrous oxides (Hylander et al., 2000).

4.2 Blirh River

4.2.1 Chronostratigraphy and morphodynamic evolution

The Blirh floodplain is also characterised by a cut-and-fill alluvial system formed throughout the Holocene, although there are several sedimentary gaps, especially from the end of the Early Holocene until the end of the Mid-Holocene (Fig. 3). The deposits formed after 5000 cal. BP are not presented here. The chronology is based on thirteen radiocarbon datings performed on charcoal and bulk organic sediment (Table 1). The alluvial formation studied here – Bli01 outcrop – is located on the western bank of the Blirh River, immediately upstream of its entrenchment into Neogene marls, and is recognisable by its Early Holocene deposits, which extend widely within the Blirh floodplain. The Blirh formation (F1) has been previously studied by Lefèvre (1985, 1989), Lefèvre and Ballouche (1991), and Limondin-Lozouet et al. (2013), and presents 29 lithopedosedimentary facies grouped into 11 sedimentary units and finally into 5 sedimentary sequences. We noticed that the stratigraphic and morphosedimentary features of the Blirh deposits share strong similarities with those of the Tab01 outcrop at Tabouda.

Above the current thalweg, the bottom of the exposure presents a 2.5-m thick coarse deposit characterised by alternating cross-bedded sandy beds and coarser beds composed of gravel and pebbles, which have been hardened by secondary precipitation of carbonates. This channel deposit indicates a high energy fluvial environment that may be related to the river channel deposit identified at the same stratigraphic position at the Tab01 outcrop, and is potentially associated with the Younger Dryas period. The first 1.5-m thick sequence analysed (S1) is characterised by yellow silts to sandy silts with a (macro-) prismatic structure. Again, the sequence is not dated, but is similar to the S1 sequence identified at Tabouda in terms of lithology and stratigraphy, and can thus be attributed to the onset of the Early Holocene. At the beginning of the sequence, low MS values decrease slightly and the sand fraction rises as the brownish-yellow unit Ia passes to the greyish-yellow unit Ib.

An apparent change in the alluvial sedimentation occurred with the transition from units BLI01-I to BLI01-II and the concomitant start of a dark-coloured prismatic and polyhedral deposit. Unit IIb, the first dark deposit identified in the formation (Fig. 3, Fig. 6) dates to 10515–11066 cal. BP (10686). It should be noted that this change happened simultaneously in the both the Blirh and Tabouda alluvial plains. This unit II marks the beginning of another sedimentary sequence (S2) composed of 2-m thick grey silts with carbonate concretions, which lasted until ca. 5000 cal. BP. Overall, the greyish units III and IV present the highest clay proportion (> 20%), very low MS values, and frequent secondary carbonate precipitations. Within this sequence, three dark deposits (BLI01-IIb, IIIb, and IVa) present relatively larger proportions of silt fractions and higher MS values. The last two layers are dated to 9918–10484 (10223) cal. BP (unit IIIb) and 9034–9477 (9312) cal. BP (unit IVa). This sedimentary sequence ends with a level made up of calcareous oncoliths that laterally correspond to reworked tufa tubes associated with an erosional surface (BLI01-V). After a presumed hiatus at the onset of the Mid-Holocene, grey sandy–silt sedimentation started to become less carbonated (BLI01-VI, Fig. 6). Unit VII is characterised by sands with reworked shells, charcoals, tufa tubes, and flint slivers, and suggests that a flood event eroded and transported reworked archaeological remains from the alluvial plain. This flood deposit is dated to 5100 cal. BP (4883–5285 cal. BP) and marks the onset of another sedimentary sequence (S3). The silty homogenous unit VIII is characterised by a change towards warmer colours, the development of iron staining, and a continuous rise in MS values.

The following unit IX is described as a new sequence (S4), and is composed of a detrital deposit at its bottom (IXa), on which pink silts accumulated (IXb). This sequence corresponds to another morphosedimentary formation clearly identified at this outcrop and within the floodplain (Fig. 3, Fig. 9, Fig. 11), which is the result of an incision-aggradation phase of river activity. These flood deposits and overbank fines probably eroded and then covered previous deposits. The silty sedimentation is dated from 2782–2958 (2876) cal. BP until at least 2124–2320 (2231) cal. BP. The last sequence (S5, units X and XI) is similar to the previous one in terms of fluvial processes, with the deposition of the coarse-grained unit Xa at its bottom, after an underlying erosional unconformity which shows the cut-off of previous sediments. Then, a quick aggradation of sandy silt (Xb) is dated to 937–1174 (1013) cal. BP, and a thin brownish pedogenic layer (granular structure with $CaCO_3$ coatings) is dated to 920–1055 (958) cal. BP.

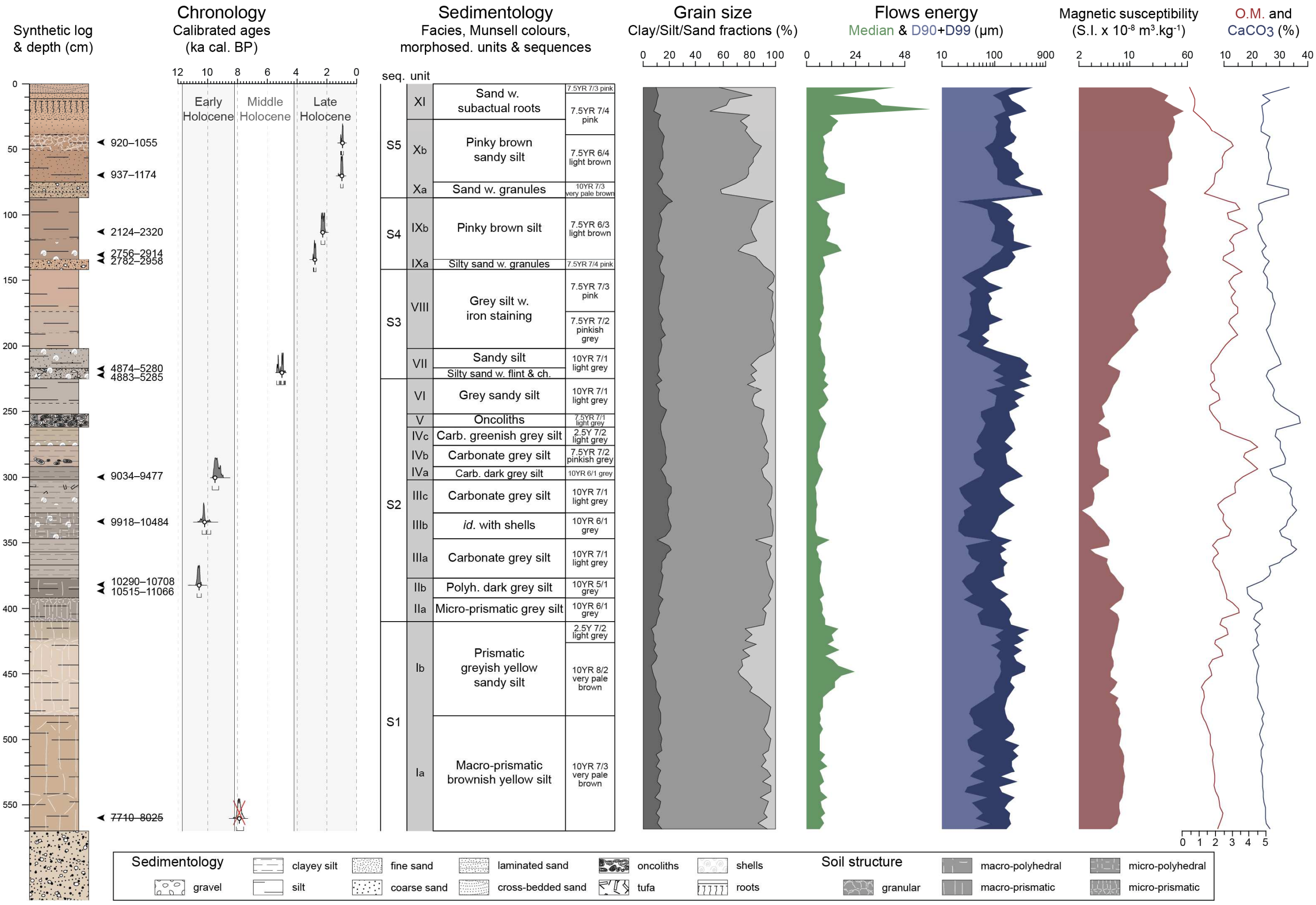

Fig. 6. Analyses of the Blirh formation – Bli01 – and its chronological features, including calibrated ages, Holocene subdivision times (after Walker et al., 2018), and sedimentological features (i.e. descriptions of facies and sedimentary units, grain-sizes from clay to sand fractions, median and coarse (90 and 99 percentiles) grain-size indices, mass-specific magnetic susceptibility, and organic matter (O.M.) and carbonate contents).

4.2.2 Palaeoecology

The following malacological data were published by Limondin-Lozouet et al. (2013), who give the full details. The Bli01 outcrop is divided into three mollusc zones (BLI01-MZ 1–3, Fig. 7). The earliest sediments are virtually unstudied, except for the last samples from BLI01 unit I (MZ 1). This first zone is dominated by hygrophilous species (ca. 50%–60%, mainly *Vallonia pulchella*, *Hygromiidae* sp. 1, or *Cochlicopa lubrica*), followed by aquatic species (ca. 40%) that indicate moist riverbanks. From ca. 10700 cal. BP onwards (BLI01 unit IIb), the proportion of aquatic species increased (mostly *Melanopsis* cf. *praemorsa* and *Mercuria similis*), forming from 50% to 90% of the total assemblage. Within this MZ 2 zone, fluctuations in the mollusc assemblage show three peaks with higher percentages of aquatic species at ca. 10500, 9800, and 9000 cal. BP, indicating enhanced and more permanent waterbodies (BLI01 units IIIa, IIIc, and IVc-V). Three other periods marked by relative increases in hygrophilous and xerophilous species demonstrate slight returns to more terrestrial and moist environments at ca. 10200, 9300, 5300-5200 cal. BP (units IIIb, IVa-b, and VI). Finally, after the coarse BLI01 unit VII, zone MZ 3 marks a clear shift in the shell assemblage with a strong reduction in aquatic species to the benefit of xerophilous species (mainly *Helicopsis verignoni* and *Truncatellina cylindrica*), hygrophilous species (mostly *Vallonia enniensis*, *Vallonia pulchella* and *Pupilla* cf. *alpicola*), and *Hygromiidae* sp2. This biozone, initially divided into six phases, indicates the overall development of terrestrial biotopes right after the flood deposit at 5100 cal. BP. Variations in the percentages of the malacological populations indicate slight environmental modifications, with unit VIII being marked by the transition from an open dry habitat to a wetter marshy environment. High amounts of *Hygromiidae* sp.2 are characteristic of a particular herbaceous shrubby vegetation colonised by this taxon. During S4, the floodplain constituted a mosaic landscape that was mostly open and dry but with persistent wet habitats because of the proximity of the river (BLI01 unit IX). The top of the sequence (S5) is characterised by an aquatic to humid environment, despite low percentages of xerophilous species (15%–30%), which is in agreement with a flood deposition period and a probable rise in the river beds (units X and XI).

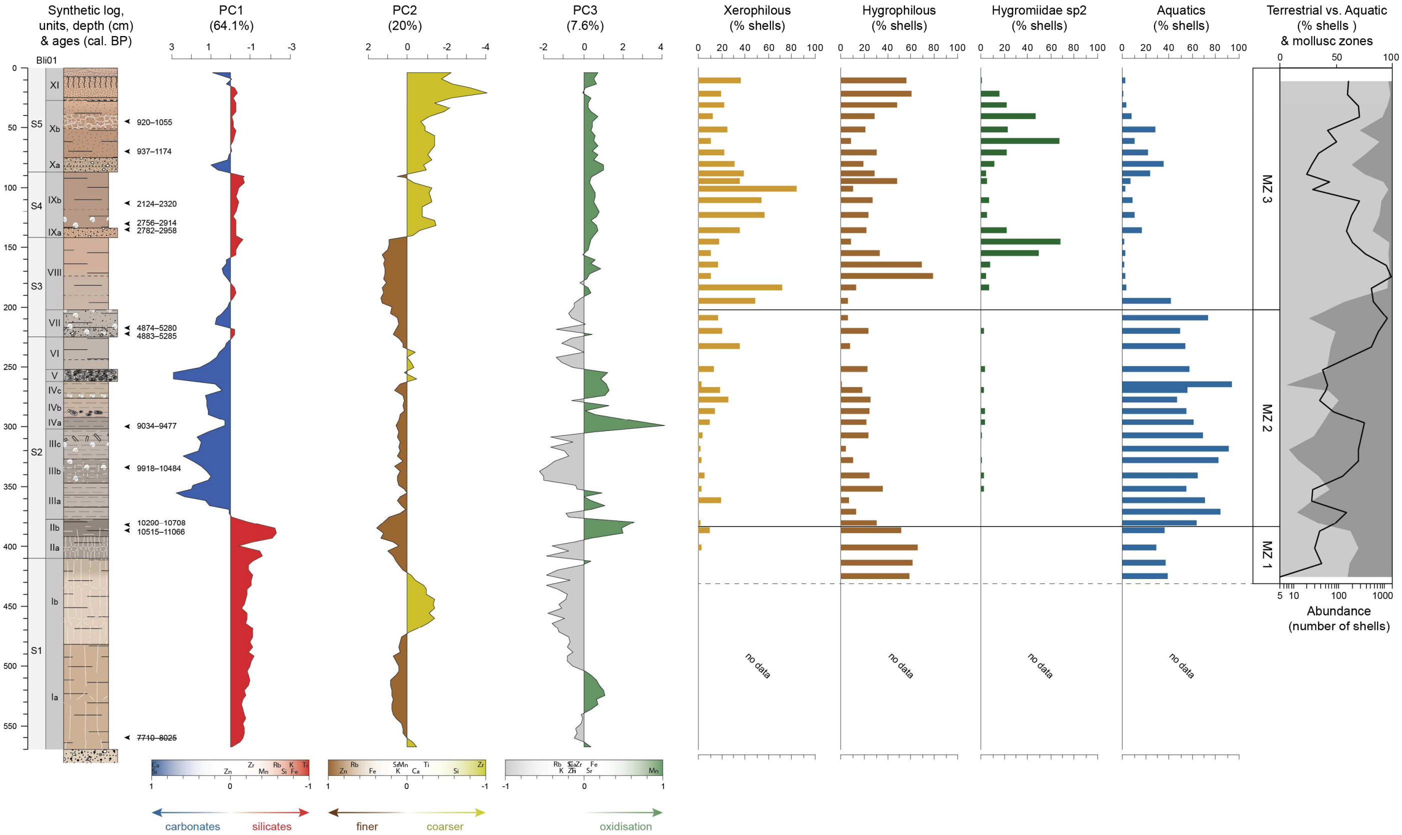

Fig. 7. Analyses of the Blirh formation – Bli01 – including the statistical results from the ED-XRF analyses, the third principal component with its correlations with the variables and their interpretations, and the malacological results (i.e. hygrophilous, xerophilous, and aquatic shell contents, and terrestrial [hygrophilous + xerophilous] vs aquatic percentages with abundance of shells and mollusc zones).

4.2.3 Geochemical proxies

4.2.3.1 Statistical features

As with the Tab01 outcrop, a PCA was conducted on the geochemical data to provide a statistical interpretation of the composition of the pedosedimentary units. The first three PCs represented 91.7% of the total variance of the data. The highest cos² values for each element were also associated with these first three components, helping to verify the quality of the data representations obtained (Table 3). The following interpretations of the PCs are supported by an AHC analysis, which showed broadly the same categories of elements as found for the Tabouda formation: Ca-Sr-Zn, Zr-Ti-Si-K, Fe-Mn, and Rb (Fig. S4).

Table 3. Principal components from the Blirh outcrop. Highest values are marked in bold.

	PC1	PC2	PC3
Variance (%)	64.07	20.03	7.65

Cumulative variance (%)	64.07	84.09	91.74
Factor/Variable correlations			
Si	**−0.676**	−0.620	−0.176
K	**−0.774**	0.116	−0.288
Ca	**0.956**	−0.112	−0.145
Ti	**−0.946**	−0.244	−0.131
Mn	−0.420	0.054	**0.886**
Fe	**−0.809**	0.442	0.129
Zn	0.036	**0.811**	−0.155
Rb	−0.590	**0.670**	−0.336
Sr	**0.964**	0.145	0.065
Zr	−0.258	**−0.932**	−0.066
Cos^2 values			
Si	**0.457**	0.385	0.031
K	**0.599**	0.013	0.083
Ca	**0.914**	0.012	0.021
Ti	**0.894**	0.059	0.017
Mn	0.176	0.003	**0.786**
Fe	**0.655**	0.195	0.017
Zn	0.001	**0.658**	0.024
Rb	0.348	**0.449**	0.113
Sr	**0.930**	0.021	0.004
Zr	0.067	**0.869**	0.004

4.2.3.2 Interpretation of the principal components

Because of the high similarity with the geochemical findings obtained from the Tabouda formation, the interpretations made here refer to section 4.1.3.2 when similar trends are revealed, but are developed further when differences are noted.

The first PC (PC1) represented 64.1% of the total variance and showed significant positive correlations with Ca and Sr, and negative correlations with the association of Ti, Fe, K, Si and Rb elements (Fig. 7). As is the case for the Tabouda outcrop, this component is strongly associated with a carbonate vs silicate content opposition. Positive scores reveal unaltered carbonate supply from the catchment, which is mostly composed of Cretaceous and Jurassic limestone, or on-site precipitation in the form of tufa deposits. To the contrary, negative scores may reveal more siliciclastic or chemically weathered deposits by pedogenic processes.

The second component (PC2) represented 20% of the variability, with Zr and Si being significantly negatively correlated, whereas Zn, Rb, and to a lesser extent Fe, were positively correlated. The interpretation of this component is similar to that for Tabouda: negative scores reveal grain-size increases interpreted as high energetic fluvial deposits (units Ib and IX–XI). This is in good agreement with geomorphological evidence, which demonstrates that the coarsest units correspond to flood deposits that cut into previous formations and resulted in sedimentary gaps (Fig. 3). Flooding processes in the Blirh and Tabouda catchments are interpreted as an aridification trend. In semi-arid to arid catchments, the climatic control of these processes has been a matter of debate (Fletcher and Zielhofer, 2013). A recent relevant synthesis of Holocene semi-arid river systems from central and southern Iberia (Wolf and Faust, 2015; Faust and Wolf, 2017), and previous relevant publications (Lefèvre, 1989; Sancho et al., 2008; Benito et al., 2015), demonstrated that flooding processes occurred under arid conditions, whereas floodplain stabilisation and pedogenesis took place under humid climatic conditions. According to biorhexistasy concepts (Erhart, 1955), climatic aridity will lead to decreasing vegetation cover and increasing runoff, as explained in section 2.1. The PC2 positive scores are driven by the association of Zn, Fe, and Rb. The first two elements have already been interpreted as indicating a fine-grained sedimentation, in opposition to a coarse-grained flood event. The behaviour of Rb in sedimentary and pedogenic processes depends on the clay and organic matter content, which explains its negative correlation with Zr on this axis. Despite the solubility of Rb^+, rubidium is characterised by low mobility, as it is readily adsorbed onto clay minerals, especially at high pH (Kabata-Pendias, 2001). Consequently, the correlation between Zn and Rb provides further evidence of an interpretation of PC2 positive scores as revealing fine-grained sedimentation.

The third axis (PC3), representing 7.6% of the variance, is positively correlated with Mn, whereas the other elements do not show any correlation. Therefore, the interpretation of high amounts of highly redox-sensitive Mn in Blirh is comparable to that for Tabouda, i.e. an oxidisation trend.

5 Discussion

5.1 Holocene morphodynamic changes in the upstream Moulouya rivers

Comparisons between the two studied outcrops highlight similarities in their morphosedimentary and chronostratigraphical evolution. They show co-occurring alluvial sedimentation at the onset of the Early Holocene, and a probable important sedimentary hiatus at the Early–Mid-Holocene transition. Differences are also noted, such as the multiple flooding events recorded in the Early Holocene sedimentation at Tabouda or the Late Holocene sedimentation at Blirh, but these are easily explained by the discontinuity characteristics of the alluvial archives or the variability of river deposits within the floodplain, which depend on the distance from the stream bed (distal or proximal position). Indeed, because of variability in fluvial architecture, one exposure cannot summarise the entire floodplain history, which will need to be completed by future studies.

Apart from these discrepancies, both study areas display coarse channel deposits linked to the first aggradation phase at the bottom of the alluvial formation. On the basis of the stratigraphical and chronological results, these can be attributed to the Late Glacial period, and potentially to the YD period. Evidence of the impacts of the YD on Moroccan landscapes have been provided by Hughes et al. (2018) in the form of the last glacier advance in the High Atlas, and by Zielhofer et al. (2017a) as a colder phase recorded in the Sidi Ali lake. Despite this evidence and the regional indices from marine cores (Cacho et al., 2001; Fletcher and Sanchez-Goñi, 2008; Combourieu-Nebout et al., 2009), the YD is still poorly known in North Africa, with there being no mention in its fluvial systems. In this context, our record suggests a period of high fluvial activity leading to an entrenchment of the river into Neogene marls, as observed at Blirh, with gravel deposition close to the current base level at both study sites.

Starting from 11700 cal. BP, the Early Holocene is marked by a reduction in fluvial energy and a rise in the lasting water table, as well as a fine and structured yellow silty aggradation of the floodplain (BLI01 and TAB01 – units I). This aggradation, spanning the first centuries of the Holocene up to 10800 cal. BP, was characterised at Blirh by Lefèvre and Ballouche (1991). Clay mineralogy and micromorphological analyses demonstrated that this sedimentation, abundant in illite, was a product of the erosion of the Neogene marls resulting from an intermittent low-energy runoff. This poorly organic sedimentary sequence (S1) is consistent with indications of a steppe marked by *chenopodiaceae,* and indicates rather arid conditions (Lefèvre and Ballouche, 1991).

The climate at the onset of the Early Holocene seems to show contrasts around the Mediterranean basin, as several studies have demonstrated enduring dry conditions inferred from south-western Mediterranean pollen records, whereas western Europe had experienced wetter conditions (Carrion, 2002; Fletcher et al., 2010; Magny et al., 2011; Combourieu-Nebout et al., 2013; Desprat et al., 2013). Considering the climatic contrasts across a north-south gradient, the first millennium of the Holocene, equivalent to the Preboreal biozone in north-western Europe, was generally drier in the southern Mediterranean (south to 40°N) than further north (Magny et al., 2013; Peyron et al., 2017). In accord with the south-western Mediterranean records, our findings document prevailing arid climatic conditions in the Moulouya basin during the 12th millennium.

The two alluvial formations demonstrated simultaneous commencement of organic and palustrine deposition at 10800 cal. BP. This simultaneous hydrosedimentary evolution of the two catchments located 300 km apart from each other suggests a climatic forcing factor, and this clear change is undeniably caused by the transition towards a wetter period. The PC1 factors show high carbonate sedimentation at Bli01 and Tab01 outcrops during the wetter period, as noticed in the Ksabi basin by Lefèvre (1985), and consistent with tufa and marshy deposits that indicate broadly humid and stable conditions within the floodplain. High proportions of aquatic shells in the mollusc assemblages of the two basins confirm this assumption. The sedimentary sequence (S2) of the Bli01 outcrop developed laterally with the in situ formation of more compact tufa deposits. Such a formation was described by Lefèvre and Ballouche (1991) at Aït Blal, another tributary of the Moulouya (Fig. 8), with it showing the downstream development of a tufa barrier across the river, behind which carbonate and organic grey silts were deposited. At Tabouda, the related sedimentary sequences (S2 to S4) from the Tab01 outcrop present some coarse deposits due to the proximal position of the profile, with these indicating persistent enhanced fluvial events leading to erosion and sand-gravel deposition. However, the presence of reworked tufa tubes at the end of the coarse deposits (Vb and VIIb units) suggest erosion of tufa formations in the stream bed. In the ABM basin, another alluvial outcrop at Châaba Bayda demonstrated in situ tufa formation and an Early Holocene palustrine environment (Fig. 8, Wengler and Vernet, 1992).

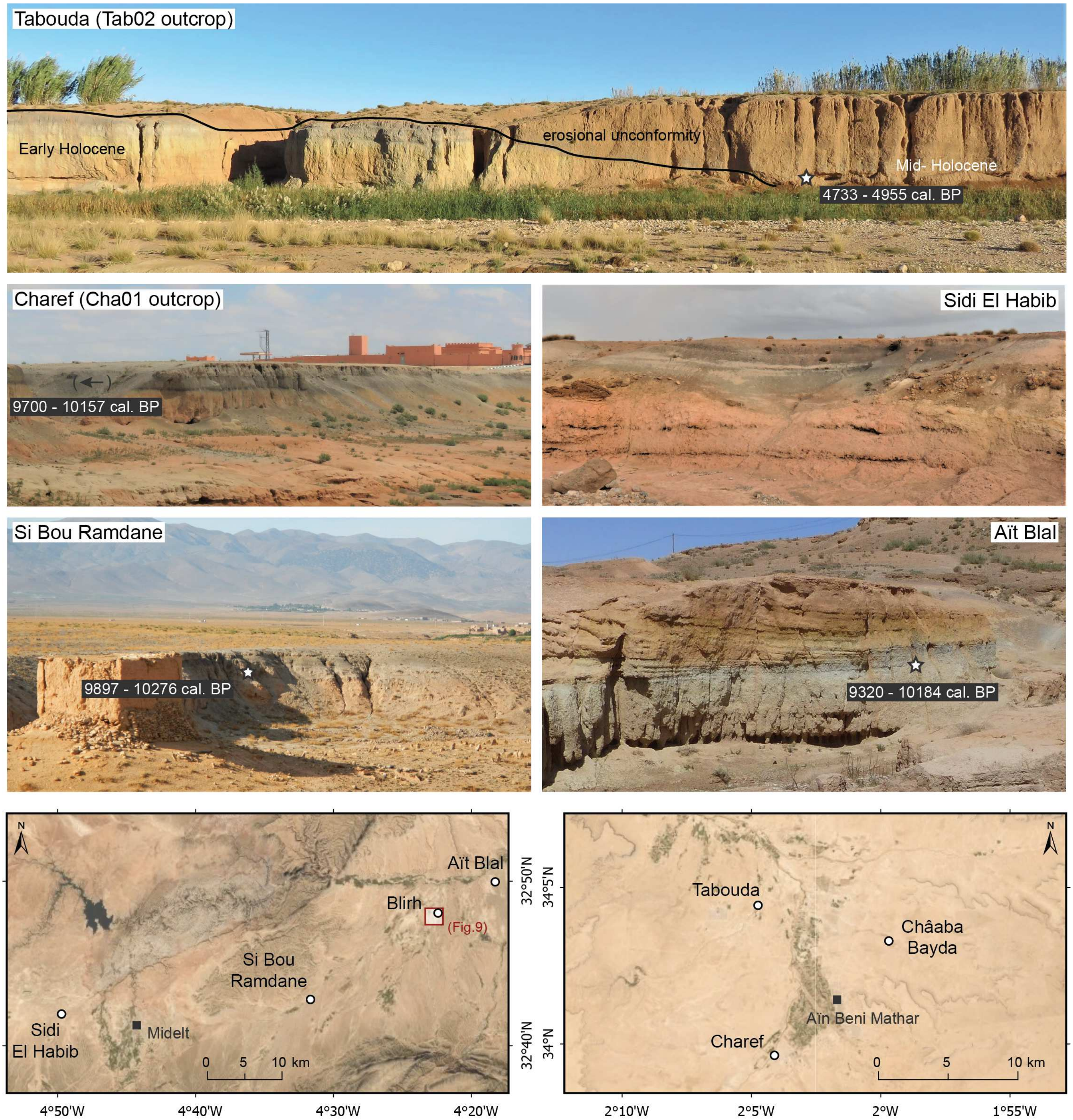

Fig. 8. Photographs of Early – Mid-Holocene alluvial deposits discovered in upper and middle Moulouya and ABM basin. Maps show satellite images with hill-shade elevation, obtained from TerraColor imagery (Esri, 2009), and localisation of the alluvial deposits (included the Châaba Bayda formation from Wengler and Vernet, 1992) and the Blirh alluvial plain in figure 9.

Indeed, as mentioned above, both sections are representative of the Early–Mid-Holocene sedimentary formations in the Ksabi and ABM basins. Other alluvial outcrops demonstrate the recurrence of this formation in upper and middle Moulouya, as evidenced by similar sedimentary facies, chronology, and stratigraphic positions (Fig. 8). These extensive Early Holocene deposits are located 5 to 10 m above the current riverbed, depending on the floodplain width and the valley incision. In the ABM basin, in addition to the Châaba Bayda outcrop, another section from the Charef River (Cha01 outcrop) displays this type of deposit, which widely extends within the alluvial plain and is characterised by similar facies and stratigraphic patterns and is dated to 8840 ± 50 BP (9700-10157 cal. BP). As already noted, the Aït Blal section in the Ksabi basin, which was studied by Lefèvre and Ballouche (1991) and dated to 8650 ± 160 (9320–10184 cal. BP), demonstrates the development of a tufa barrier in tributaries downstream near the confluence with the Moulouya River at that time. In its upstream part, the Si Bou Ramdane section also presents fine grey deposits in an elevated floodplain position dated to 9000 ± 70 (9897–10276 cal. BP). Such formations have even been identified in the upper Moulouya, e.g. in the Sidi El Habib wadi (Fig. 8). Moreover, satellite images show the substantial area of this formation within the studied alluvial plains, and in the case of the Blirh River, they show that a major part of the floodplain preserves this formation across its width (Fig. 9). This supports the view of the extension of hydromorphic features interspersed with darker deposits through the alluvial plain, and the development of more palustrine conditions with tufa sedimentation in a proximal position near to the river stream. These conditions may have resulted from a high groundwater level and indicate stable and wetter climatic conditions.

This formation lasted for several millennia until the middle of the Mid-Holocene, with its termination not appearing to be simultaneous in both studied outcrops, but presenting a time lag of over a thousand years. Taphonomic factors may be taken into account, as there are discrepancies in the preservation of fluvial records because of the early Mid-Holocene entrenching of river systems (ca. 8000-6000 cal. BP), entrenching of river systems is supposed here owing to the sedimentary hiatuses in the studied outcrops and field survey observations in both basins. Indeed, the Bli-01 and Tab-01 outcrops do not show clear indices of sedimentation during the 9–6.5 cal. ka interval. Coarse units and erosional unconformities at Blirh and Tabouda (Fig. 2, Fig. 3, Fig. 8) tend to demonstrate that post incision-aggradation coupled processes removed Early–Mid-Holocene deposits at different times. These processes are illustrated by the Tab02 outcrop, where the Early–Mid-Holocene formation (F1) was incised, and sandy gravel deposits then cohesive overbank fines started to accumulate from ~5000 cal. BP (F2). This later outcrop reveals an example of an incision-aggradation cycle that may have occurred previously during the Early–Mid-Holocene, as implied by the sandy-gravel deposits at S3 or S4 in the Tab01 outcrop. At Blirh, we assume that the sedimentary gap during the first part of the Mid-Holocene resulted from at least one incision phase. This phase is indicated by several indices of erosional unconformities (Fig. 8), and has been widely identified elsewhere in the alluvial plain.

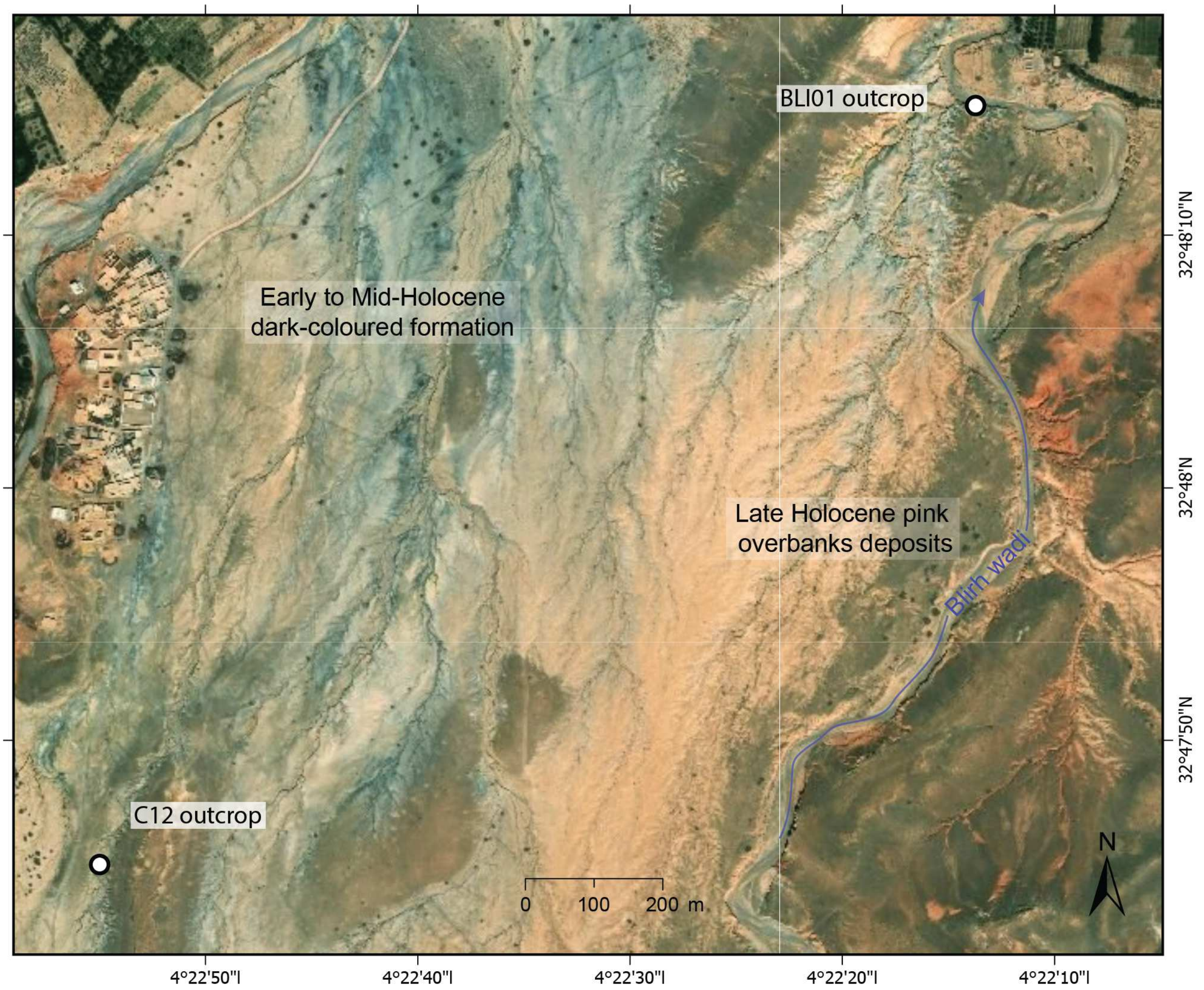

Fig. 9. Satellite image of the Blirh alluvial plain, showing the large extension of Early – Mid-Holocene silty formation which were covered by Late Holocene pink overbank silty to fine sandy deposits. The satellite images were obtained from TerraColor imagery (Esri, 2009).

Concerning the end of the palustrine conditions, chronological data from the Tab01 outcrop indicate that the humid floodplain still prevailed until ca. 6200 cal. BP, although it was interrupted by several periods of flooding events during the Early Holocene and early Mid-Holocene. The end of this period is marked by a trend towards a more terrestrial environment supported by a palaeoecological and geochemical shift at the S4–S5 transition (Fig. 5). At Blirh, the termination of palustrine conditions at ca. 5100 cal. BP was also characterized by a hydrosedimentary and palaeoecological shift at the S2–S3 transition (Fig. 7). The deposition of a coarse deposit including charcoals and flint slivers indicates high fluvial dynamics and erosion of the Neolithic settlements located in the alluvial plain. This event may potentially be related to Tab01-S6, showing that a strengthened fluvial phase occurred a while after 5400 cal.

BP, and could reflect a more regional signal, as a transition from floodplain stability towards aggradation was observed at ca. 5000 cal. BP in southern Iberian river catchments (Wolf and Faust, 2015).

These data suggest a fluvial tipping point associated with the climatic aridification widely identified in the Mediterranean and North Africa (Fletcher and Zielhofer, 2013). This view is supported by the last sedimentary sequences of both studied outcrops. As mentioned above, cohesive overbank fines (S5–S6) were deposited in an elevated floodplain position in the Tab01 outcrop, whereas the river entrenched at a height of more than 5 m then started to aggrade again at ca. 5000 cal. BP in the Tab02 outcrop (Fig. 8). These findings suggest a morphogenic change in the river system characterised by the incision of an older sediment sequence and the formation of a new one.

In a similar way, the S3 to S5 sedimentary sequences from the Bli01 outcrop display clear floodplain deposits from the end of the Mid-Holocene and the Late Holocene, marked by sandy flood deposits at the bottom, suggesting strengthened flooding events potentially associated with incision phases. Subsequent brownish silty deposition indicates an aggradation of the floodplain with cohesive overbank fines. The last two dates indicate that a terminal flooding event (S5) occurred ~1000 cal. BP. This flood deposit, located in a more distal position, corresponds laterally to a 2–3-m-high gravel deposit at the east of the alluvial plain (F2, Fig. 3) that cuts off all previous sediments. Hence, in this part of the floodplain, no Early to Mid-Holocene deposits have been found. This event could indicate an important hydrosedimentary change characterised by river incision and high discharge that occurred at ~1000 cal. BP. Following this, the base level decreased again and the F3 low terraces were deposited.

5.2 Regional fluvial evolution during the Early to Mid-Holocene in NE Morocco

Analyses of the Tab01 and Bli01 formations demonstrate clear similarities in terms of morphosedimentary and chronostratigraphical evolution throughout the Holocene. In the Moulouya highlands, floodplain aggradation started under arid conditions at the onset of the Early Holocene, with wetter conditions then prevailing during the Early–Mid-Holocene with the formation of wetlands in the alluvial plains. These conditions stopped in the course of the 6–5 ka interval, with a probable fluvial tipping point leading to morphogenic changes. As noticed in many outcrops, several incision-aggradation cycles that removed previous deposits occurred during the Mid to Late Holocene. When

Early Holocene formations are preserved, they show the same sedimentary facies and topographic position in the alluvial plain. If similar patterns are shown for rivers in the Moulouya highlands, it can be asked “what are the river responses to Holocene climatic changes on a more regional scale”?

Fifty-two radiocarbon dates have been compiled from NE Moroccan fluvial studies performed over past decades. Apart from Wengler’s work in the ABM basin, the works were conducted downstream in the lower Moulouya (Zielhofer et al., 2010; Bartz et al., 2017), in the Kert River (Barathon et al., 2000; El Amrani et al., 2008; Zielhofer et al., 2008), and in the Isly basin (Wengler and Vernet, 1992; Wengler et al., 1994). Thus, one of the main points of interest is a comparison of the hitherto unseen upstream Moulouya archives with the downstream river studies in coastal areas, which is all the more important because very few studies have been performed in the SW Mediterranean.

Comparisons with NE Moroccan alluvial formation chronologies highlight that the Early Holocene deposits have been documented almost exclusively in the upstream part of the Moulouya basin (Fig. 10). Indeed, a few dates performed in the Kert basin revealed deposits encompassing 9300–8700 cal. BP (El Amrani et al., 2008; Zielhofer et al., 2008). Alluvial deposits from this time may not be well preserved in the upstream sections of the Moulouya basin because of post-incision phases. Ibouhouten et al. (2010) also document Early Holocene deposits ca. 9600-9900 cal. BP at the bottom of the Djamila outcrop near the current base level. Apart from these dates, only upstream sections such as the Blirh and Tabouda outcrops display preserved Early Holocene sedimentary formations deposited since at least 11500 cal. BP. As mentioned in section 5.1, another alluvial deposit from the ABM basin (Châaba Bayda outcrop) revealed several dates from that time (Wengler and Vernet, 1992), and several sections from our field surveys (i.e., in the Charef, Aït Blal, Si Bou Ramdane, and Sidi El Habib rivers) display extensive Early Holocene deposits (Fig. 8). Further downstream, chronologies of other alluvial records indicate a sedimentary gap at that time (Fig. 10). This upstream-downstream discrepancy might result from connection of the base-levels of the coastal rivers with the Holocene sea-level rise. Indeed, most of the NE Moroccan alluvial studies discussed here are located less than 40 km from the sea (lower Kert or Moulouya valleys). During the Early Holocene, the level of the western Mediterranean Sea rose rapidly from approximately −45 m to −15 m lower than today (Vacchi et al., 2016). Alluvial sedimentation from that time was probably eroded or covered by recent deposits. In this sense, these studies exhibit recent deposits characterised by an important thickness, e.g. the 10-m-thick Late Holocene Djamila sequence. To the contrary, the base-levels of the upstream rivers could not vary with sea-level given the many knickzones along the Moulouya basin, e.g. the Beni Snassen, the Oujda Mounts, and the Tamdafelt gorges.

In addition, it should be noted that a few dates, marked by high 2-sigma standard deviation, suggest potential preservation of Late Glacial deposits in the Kert and Lower Moulouya areas (Fig. 10). These deposits are more precisely dated between 13 and 15 ka cal. BP, equivalent to the Bølling-Allerød warming, and are characterised by a dark-coloured organic silty sediment and tufa deposits (Barathon et al, 2000; El Amrani et al., 2008). These indices, which indicate wetter climatic conditions, suggest that similar Early–Mid-Holocene wetland environments, which developed along valley bottoms, may have started at the onset of the Late Glacial period. In this case, the lack of such deposits in our records could be explained by the coarse channel deposits linked to an erosive activity identified at their base, which are potentially attributed to the YD period. Wengler et al. (1992) also present two radiocarbon dates of ca. 13 ka cal. BP from the base of the Châaba Bayda outcrop. However, one must be careful in interpreting these dates, as they were realised on different materials, including ostrich eggs, and no calibration studies have been performed to assess the relevance of such dating material. For example, at the Charef River, the Early Holocene dark deposit corresponding to the Cha01 outcrop that we dated at 8840 ± 50 (Fig. 8), was dated at 12120 ± 170 using total organic matter (Wengler and Vernet 1992).

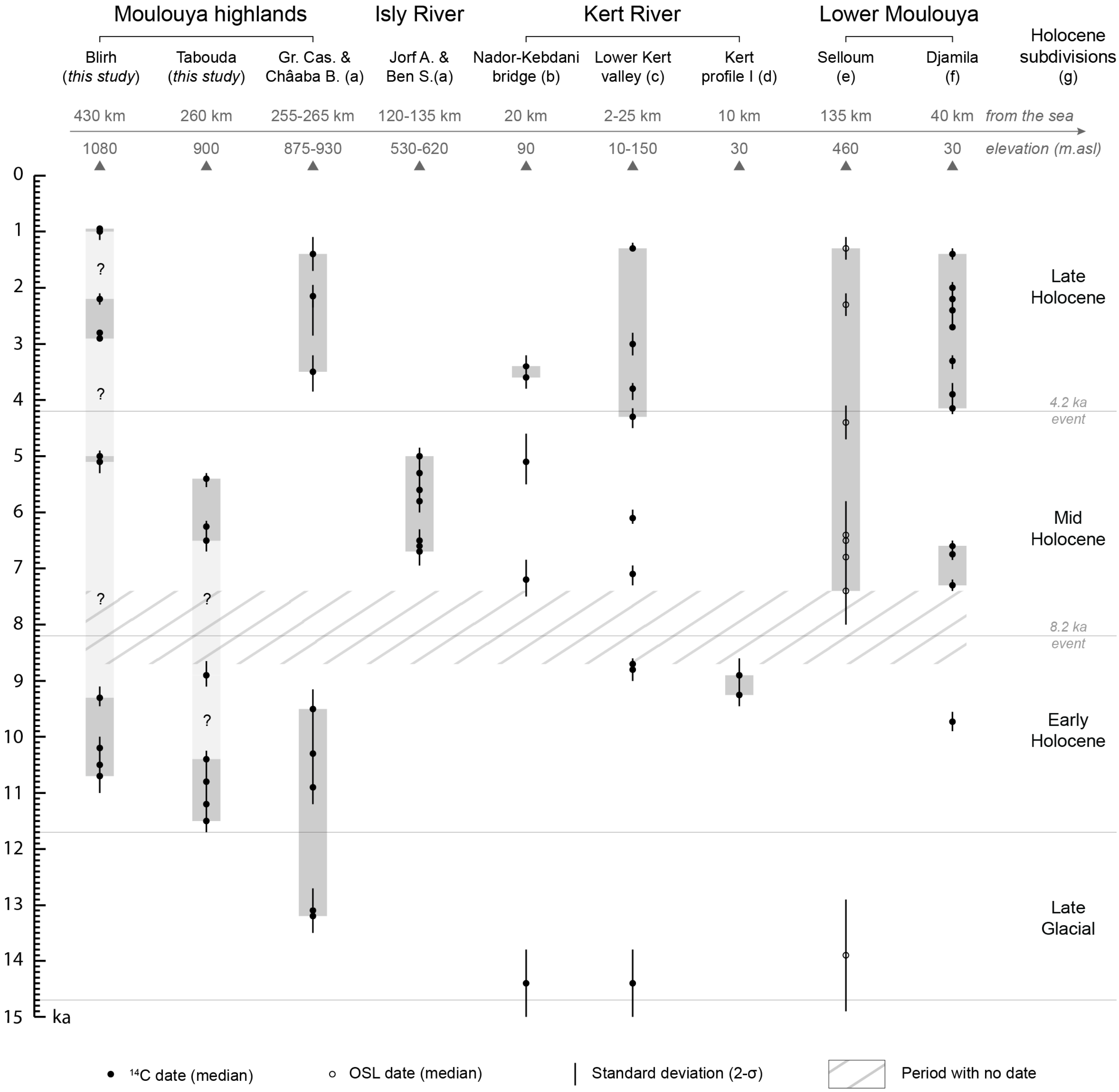

Fig. 10. Comparison of alluvial formation chronologies of the upstream studied river sections (Tabouda and Blirh) with other fluvial studies from NE Morocco: the El Hay River and Isly River ((a) Wengler et al., 1994); Kert River ((b) Barathon et al., 2000, (c) El Amrani et al., 2008, (d) Zielhofer et al., 2008); and lower Moulouya River ((e) Bartz et al., 2017, (f) Ibouhouten et al., 2010 and Zielhofer et al., 2010). Vertical grey bars indicate continuous sedimentary formation with successive radiocarbon dates. Vertical light grey bars concerning the Tabouda and Blirh outcrops are taken into account possible sedimentary hiatuses. Holocene subdivisions refer to Walker et al., 2018 (g).

At the Early–Mid-Holocene transition, the sedimentary hiatus identified at Blirh and Tabouda dating from between ca. 9 and 6.5 ka cal. BP is reflected in the lack of sedimentary formations from other alluvial studies in NE Morocco.

At the minimum, all NE Moroccan alluvial deposits record a common sedimentary gap between 8.7–7.3 cal. BP (Fig. 10). No explanation has yet been proposed for this issue. One could postulate that the global-scale 8.2 ka event may have affected Moroccan river systems, but as already noted by Zielhofer et al. (2008), no alluvial archives from the SW Mediterranean display a clear record of this event.

Another issue is the alluvial sedimentation during the last millennium. Indeed, the NE Moroccan studies display a common lack of sedimentary deposits from this interval. Only Barathon et al. (2000) present an isolated date of 550 ± 45 BP, which is from a 2-m-high silty deposit near Tafersite in the Kert basin. Within the studied formations, the last two dates from the Bli01 outcrop indicate the occurrence of a terminal flooding event (S5) at ~1000 cal. BP. As seen in section 5.1, this event is interpreted as an important hydrosedimentary change characterised by river incision and gravel aggradation and occurred ~1000 cal. BP. Following this event, the base-level decreased, with recent low terraces formed during the last millennium being identified within the stream bed (F3 in Blirh, F4 in Tabouda), but no dating material having been found. The assumption of a widespread base level decrease throughout the Moulouya basin since ca. 1000 cal. BP needs to be confirmed, but would partly explain the weak representation of sedimentary deposits from the last millennium.

Apart from these general trends, changes at higher temporal resolution may be discussed. In the course of the Early Holocene, several dark fine deposits were recognised in our alluvial records (Fig. 11). These dark deposits are characterised by hydromorphic and vertic properties, such as polyhedral and prismatic sediment structure due to swelling and shrinkage of clays, and indicate seasonality in the water regime. These layers were first identified by Lefèvre and Ballouche (1991), who showed high smectite content in the clay mineralogy at Blirh. They also pointed out high organic content resulting from charcoals of herbaceous and shrub communities that were crushed into flakes or powder. These data are consistent with vertic features and malacological results indicating a rise in xerophilous and hygrophilous species in these specific deposits. The tabular form of this deposit, observed all along the studied exposures (Fig. 11) and extending throughout the alluvial plain (Fig. 9), is an additional indication of an alluvial wetland marked by high seasonal variability.

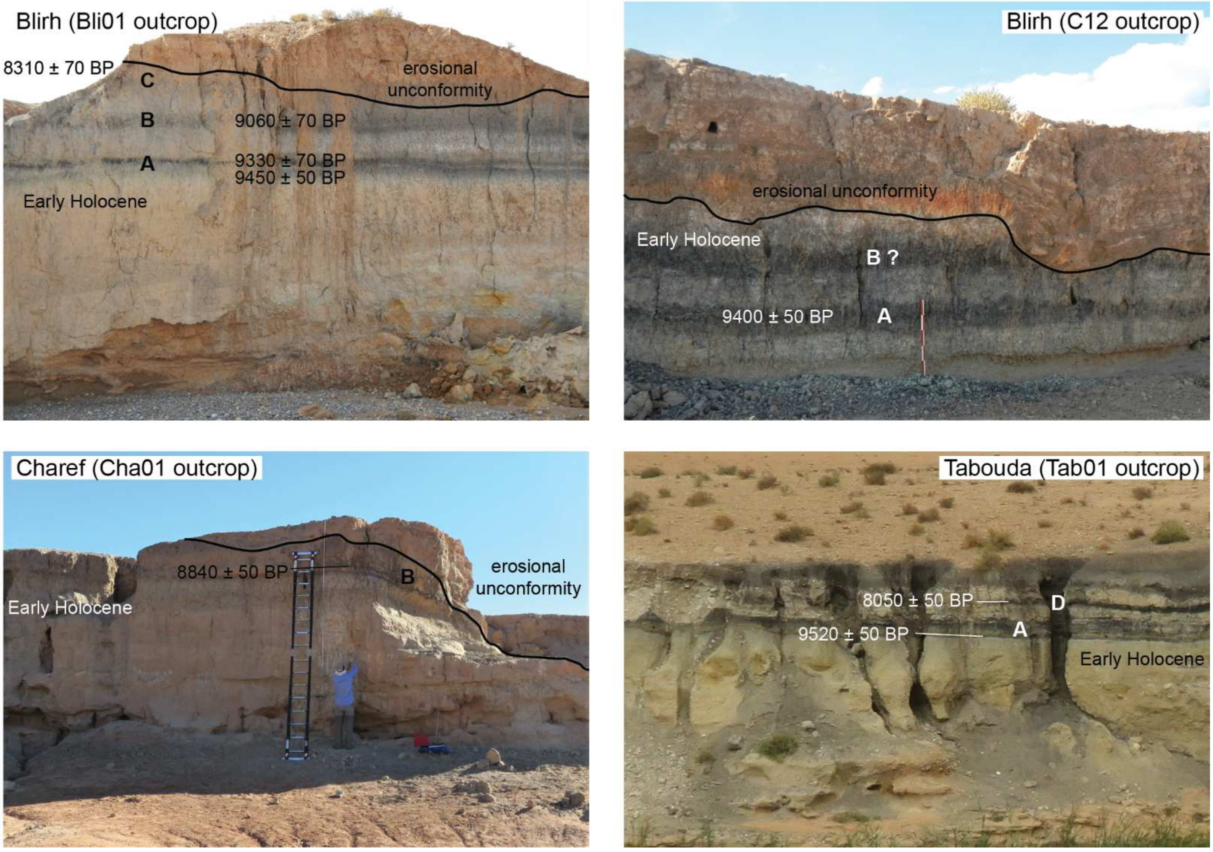

Fig. 11. Photographs of Early – Mid-Holocene alluvial formation showing successive dark deposits at Blirh, Tabouda, and Charef Rivers.

Furthermore, Zielhofer et al. (2008) highlight two similar and successive dark layers in the Kert basin, described as Ah horizons dated at ca. 9300 and 8900 cal. BP and separated by a flood deposit. Overall, six alluvial formations from the Blirh, Si Bou Ramdane, Tabouda, Charef, and Kert Rivers have given eleven radiocarbon dates performed directly on these deposits (Fig. 12). Comparisons of these radiocarbon dates and the stratigraphic succession of the dark layers reveal good synchronisms between the different basins. Indeed, four distinct horizons appear to be synchronous across the Moulouya basin. This simultaneity suggests four particular phases of geomorphic stability (A to D) dated to approximately 10800–10500, 10200–9900, 9300, and 8900 cal. BP (Fig. 12). All the phases are determined by at least two dates from two different catchments at a distance of 150 to 300 km apart. Radiocarbon dates from the lower Kert valley are perfectly in phase with those from the Blirh and Tabouda outcrops (phases C and D). Phase A is covered by four dates from Tabouda and two outcrops at Blirh. The date from the Tab-01 outcrop is a little bit older because the sample is situated in the first centimetre of the unit, which is particularly dilated in this part of the exposure. Nevertheless, phase B is less certain, with three dates that match moderately but with overlapping standard deviation. Taphonomic conditions such as the post-depositional processes must be taken into account when evaluating the preservation of these horizons within the alluvial plains. At Blirh, the first three successive horizons are visible on several profiles (Fig. 11), but the last horizon is missing and may be explained by a post-incision phase. This is also the case for the Cha-01 outcrop where a fluvial deposit eroded the Early Holocene formation. At Tabouda, only phases A and D are preserved. The lack of intermediate phases may result from the erosive coarse unit V, which underlies a possible sedimentary gap.

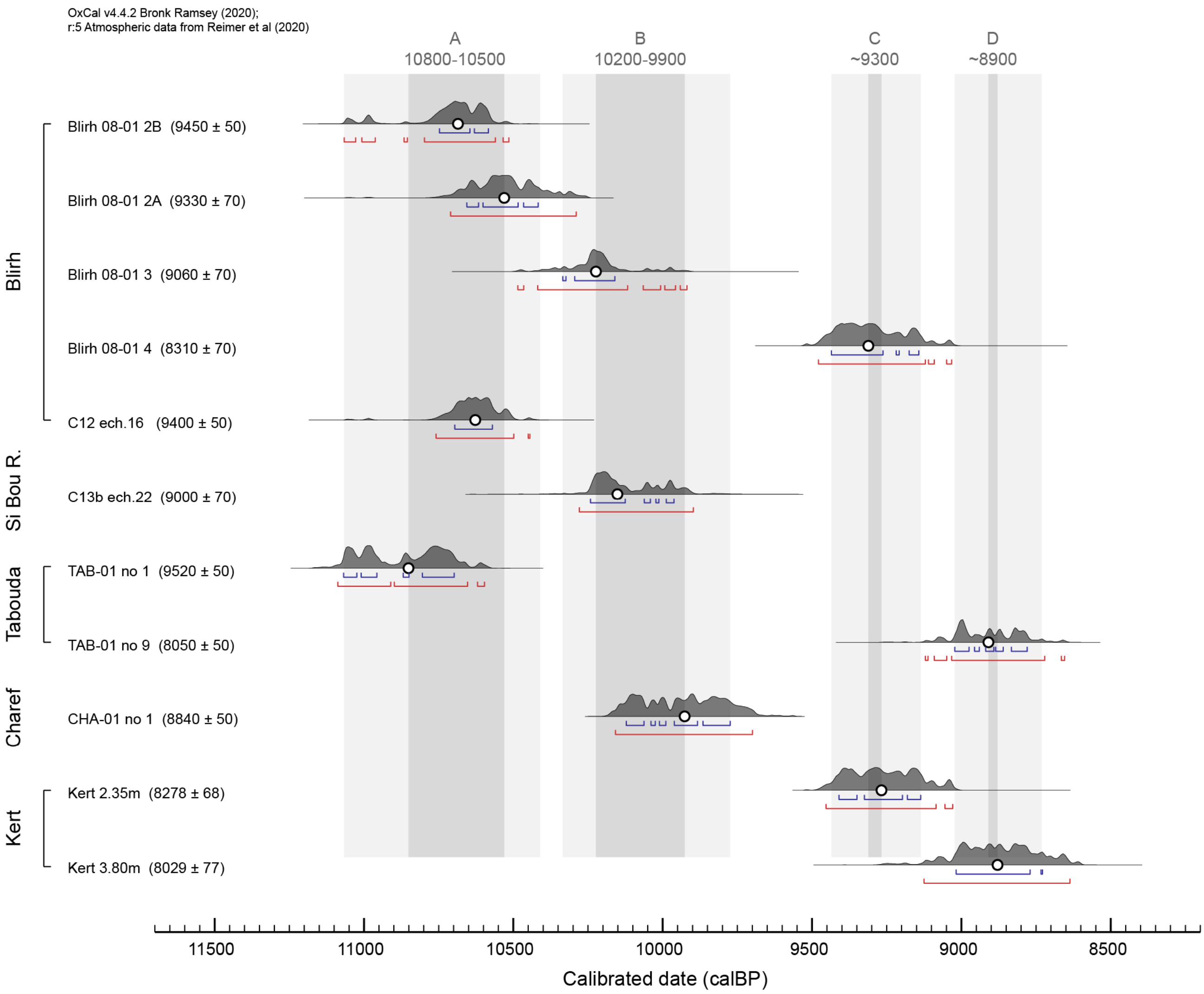

Fig. 12. Radiocarbon dates performed directly on the dark deposits from six alluvial formations at Blirh, Si Bou Ramdane, Tabouda, Charef, and Kert Rivers. Dates performed in the Kert River section (Kert I profile) are taken from Zielhofer et al., 2008. Blue bars indicate 1σ errors, red bars indicate 2σ errors.

Interestingly, this Tab01-V unit indicates a flooding phase covered by a dark deposit dated at 8900 cal. BP (phase D). This is in good agreement with the Kert River, where a flood deposit separated the two dark horizons dated at 9300 and 8900 cal. BP (phases C and D, Zielhofer et al., 2008). This similar pattern suggests a simultaneous flooding phase between the two basins after 9300 cal. BP, which indicates drier conditions. This phase may correlate with the centennial-scale cold event inferred from vegetation or SST changes in the west-central Mediterranean marine records, i.e. forest decline and APC6 phases in the Alboran Sea (Fig. 13, Fletcher and Sanchez-Goñi, 2008; Combourieu-Nebout et al., 2009) and the Siculo-Tunisian Strait (Desprat et al., 2013), which are related to the 9.2 ka cal. BP event.

5.3 Early to Mid-Holocene wetland and timing of the AHP in NW Africa

This wetland formation, not represented in other NE Moroccan rivers, occurred between ca. 10.8 to 6–5 cal. ka BP in the mid-Moulouya and the High Plateaus region in the NW African highlands. At that time, the alluvial plains displayed extensive flat organic sedimentary deposits indicating the development of a palustrine environment and tufa sedimentation, sometimes with the formation of tufa dams associated with coexisting marshes and low-energy stream channels (Lefèvre and Ballouche, 1991; Limondin-Lozouet et al., 2013).

This wetland formation was concomitant with the last AHP or the so-called "green Sahara" period defined by wetter conditions over North Africa, despite variability in intensity, timing, and extent. This humid interval started after the Heinrich event 1, simultaneous with the Bølling-Allerød warming at 14.8 ka cal. BP (deMenocal et al., 2000b; Shanahan et al., 2015), although some authors indicate a later onset at 11.7 ka cal. BP after the YD cold event (McGee et al., 2013; Tierney et al., 2017). It is a matter of debate as to whether the termination of the AHP was abrupt or progressive, but it seemed to end at ca. 5.5–5 ka cal. BP (Shanahan et al., 2015).

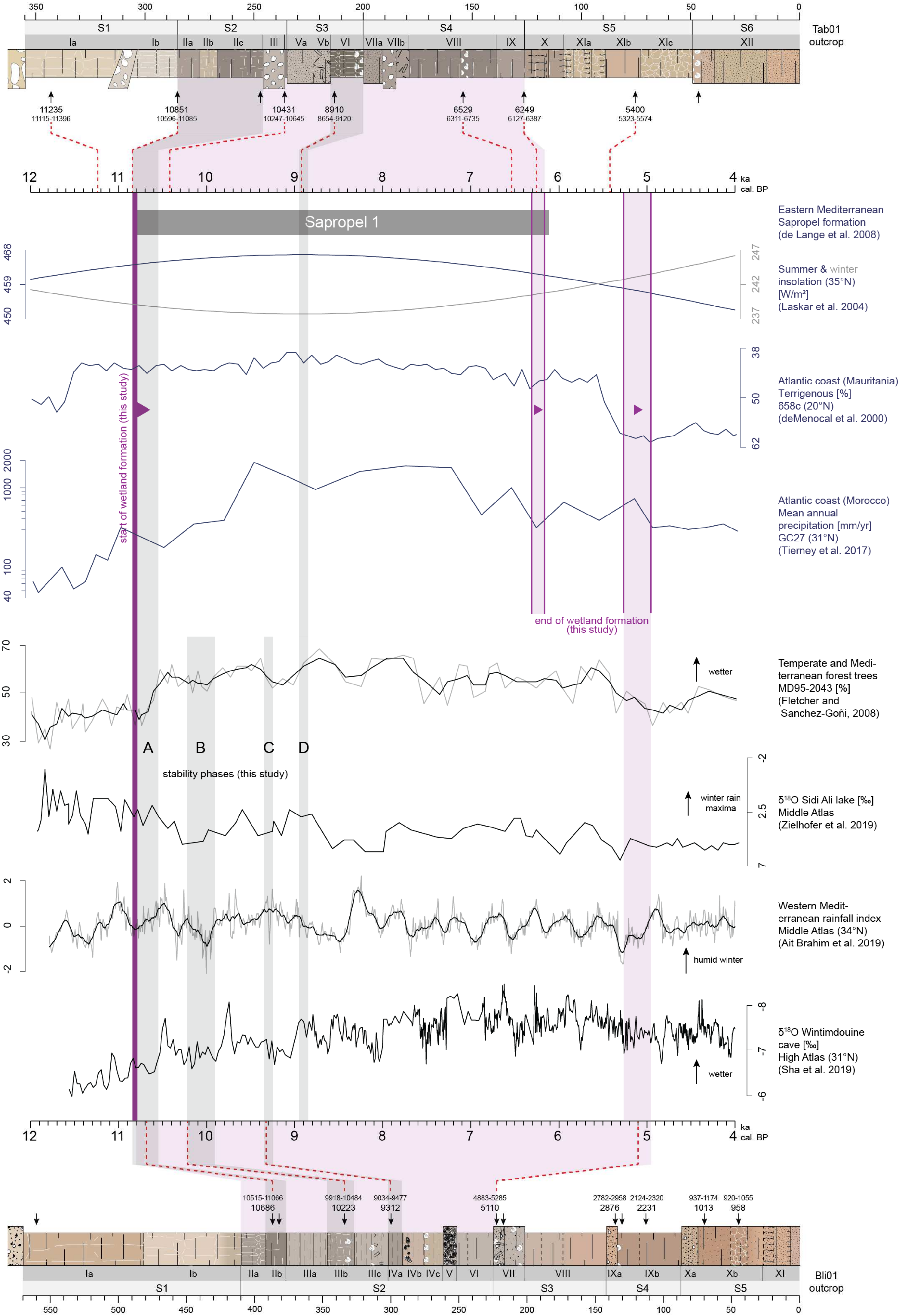

Tab01 outcrop
S1 S2 S3 S4 S5 S6
Ia Ib IIa IIb IIc III Va Vb VI VIIa VIIb VIII IX X XIa XIb XIc XII
11235 11115-11396
10851 10596-11085
10431 10247-10645
8910 8654-9120
6529 6311-6735
6249 6127-6387
5400 5323-5574
ka cal. BP
Sapropel 1
Eastern Mediterranean Sapropel formation (de Lange et al. 2008)
Summer & winter insolation (35°N) [W/m²] (Laskar et al. 2004)
Atlantic coast (Mauritania) Terrigenous [%] 658c (20°N) (deMenocal et al. 2000)
Atlantic coast (Morocco) Mean annual precipitation [mm/yr] GC27 (31°N) (Tierney et al. 2017)
start of wetland formation (this study)
end of wetland formation (this study)
Temperate and Mediterranean forest trees MD95-2043 [%] (Fletcher and Sanchez-Goñi, 2008)
wetter
A B C D
stability phases (this study)
winter rain maxima
δ18O Sidi Ali lake [‰] Middle Atlas (Zielhofer et al. 2019)
Western Mediterranean rainfall index Middle Atlas (34°N) (Ait Brahim et al. 2019)
humid winter
δ18O Wintimdouine cave [‰] High Atlas (31°N) (Sha et al. 2019)
wetter
10515-11066 10686
9918-10484 10223
9034-9477 9312
4883-5285 5110
2782-2958 2876
2124-2320 2231
937-1174 1013
920-1055 958
Ia Ib IIa IIb IIIa IIIb IIIc IVa IVb IVc V VI VII VIII IXa IXb Xa Xb XI
S1 S2 S3 S4 S5
Bli01 outcrop

Fig. 13. Comparison of the wetland formation and rapid palaeoenvironmental changes timing from the Moulouya basin with Atlantic, Mediterranean, and Saharan climatic records. At the top: solar and AHP records. Purple bars: timing of the Moulouya wetland formation. At the bottom: Western Mediterranean proxies showing centennial-scale variations. Grey bars: stability phases.

To discuss the timing of the AHP, we use the δD_p-inferred precipitation proxy from the African margin GC27 core site (Fig. 13), which was recently published by Tierney et al. (2017). Located at 31°N, it is the site off the western African coast that is closest to our fluvial archives (32°–34°N). Indeed, because of monsoonal balance, the start and end of the AHP are considered to be time-transgressive throughout North Africa, depending largely on a latitudinal trend (Shanahan et al., 2015; Tierney et al. 2017; Dallmeyer et al., 2020). Therefore, the spatiotemporal extent of these wet conditions varied from lower latitudes to higher latitudes in accord with the northward migration of the monsoon rain belt, i.e. monsoon rains started later and reduced first in the northern Sahara, because of enhanced moisture advection from the Atlantic (Bosmans et al., 2012). Such considerations are needed to explain possible time lags between different archives when considering the temporal limits of the AHP, as they are for marine records from the west African coast (deMenocal et al., 2000b; McGee et al., 2013; Tierney et al., 2017). At 20°N, AHP wet conditions increased after the YD event (deMenocal et al. 2000b), whereas at 31°N, precipitation began to increase from 11000 cal. BP (> 300mm/yr), reaching a rainfall maxima during the 9600–7000 cal. BP period (Tierney et al., 2017). These records are consistent with our data demonstrating a simultaneous onset of the palustrine environment throughout the Moulouya basin at 10800 cal. BP, which required an enhanced precipitation supply after arid conditions prevailed during the first millennium of the Early Holocene. Likewise, among the few high-latitude AHP records, the northernmost Saharan palaeolakes (i.e. Hassi el Mejnah [31.6°N] and Sebkha Mellala [32.2°N]) registered an abrupt shift from arid conditions towards a lacustrine environment at ca. 10500 cal. BP, indicating a late hydrological optimum at higher latitudes, even if the low chronological resolution based on inorganic calcite and mollusc shells is taken into account (Fontes et al., 1985; Gasse et al., 1990; Gasse, 2002). More recently, Callot and Fontugne (2008) also demonstrated that the first evidence of the lacustrine deposition in the north-eastern part of the Great Western Erg (32°N) started at 10500 cal. BP, with a maximum in the humid period between 9500-7300 cal. BP, which is consistent with the maximum of the lake extensions in North Africa (Lézine et al., 2011) and the rainfall maxima observed by Tierney et al. (2017). The sapropel deposition in the Mediterranean, particularly in the eastern Mediterranean, provides further evidence of the impact of the African monsoon on the high-latitude domains. The orbitally-driven summer insolation maxima and monsoon variations over the last 8 million years, which caused the so-called "green Sahara" periods, correspond closely to the eastern Mediterranean sapropel formation (Larrasoaña et al., 2013; Rohling et al., 2015). During the Holocene, the S1 sapropel deposition from 10800 to 6100 cal. BP was coincident with enhanced freshwater influx into the eastern Mediterranean, which was partly attributed to monsoon-driven Nile River discharges resulting from a northward monsoon migration on its headwaters (De Lange et al., 2008; Revel et al., 2010; Weldeab et al., 2014; Rohling et al., 2015). It is interesting to note that the durations of the wetland formation in the Moulouya floodplains and the S1 sapropel deposition are in good agreement (Fig. 13).

Consideration of these high-latitude AHP records of North Africa does not quite solve the question of the northernmost extent of the monsoon rains. Recent model simulations taking vegetation and dust concentrations into account have demonstrated that Mid-Holocene atmospheric conditions (at 6 ka cal. BP) allowed monsoon precipitation to extend up to 30°–35°N (Bosmans et al., 2012; Pausata et al., 2016), even up to the SW Mediterranean coast (Gaetani et al., 2017). In accord, other Mediterranean simulations suggest that summer precipitation was enhanced over the Moroccan and Algerian highlands during the Early and Mid-Holocene, although this might be considered a model artefact (Brayshaw, et al., 2011; Peyron et al., 2017), and it appears unlikely that direct monsoon precipitation reached the south-eastern Mediterranean coast (Brayshaw et al., 2011). As regards the sedimentary archives, Gasse (2002) stated that carbonate-oxygen isotope studies of the moisture signature of the northern Saharan palaeolakes at 31°–32°N show no influence of monsoon rains, but rather demonstrate precipitation originating from the Saharan Atlas Mountains. However, the author reminds us that little is known about the isotope composition of rainfall at these latitudes. A recent High Atlas speleothem record located on the Atlantic coast (Wintimdouine cave, 31°N) provided new insights into the northern extent of the west African monsoon (Sha et al., 2019). Comparisons with the Middle Atlas speleothems (34°N) highlight that both records are impacted by the NAO pattern, and that this part of the High Atlas underwent wet conditions. The authors suggest that these conditions were probably linked to the northward migration of monsoon rains, and thus assumed that the monsoon fringe did not extend further north than 34°N during the last AHP (Sha et al., 2019). These data tend to confirm that the extent of the west African monsoon was limited in NW Africa, but also reveal the ambiguity in the Early to Mid-Holocene moisture origin of this region, which was also influenced by Atlantic and Mediterranean air masses. In this respect, we assume that the Moulouya wetland formation is associated with the northern AHP record, and may be considered a counterpart to the northern Saharan palaeolakes on the other side of the High Atlas. As for the AHP lacustrine records, there is no evidence of monsoon rainfall supplies, but they might have been affected by subtropical low-latitude mechanisms in the past AHP, while westerlies and Mediterranean troughs have surely provoked winter to spring precipitation.

The wetland formation in the Moulouya basin starting at 10800 cal. BP matches the pollen-inferred forest development that occurred at 10600 cal. BP according to the Alboran Sea record (Fletcher and Sanchez-Goñi, 2008). Indeed, the Moulouya basin is the only great river flowing into the Alboran Sea; otherwise, many coastal rivers that originate from the Rif (on the south side) and Baetic (on the north side) Mountains provide important river supplies. With the Atlantic input, the MD95-2043 (or ODP 976) Alboran Sea records depict standardised signals from both Atlantic and Mediterranean influences, and thus reflect a regional afforestation trend for the western Mediterranean ca. 10600 cal. BP.

At a regional scale, the Middle Atlas pollen records do not provide a uniform response to Holocene climate variations, as certain studies show the persistence of dry conditions during the Early Holocene (Cheddadi et al., 1998; Nour el Bait et al., 2014; Tabel et al., 2016), whereas the most recent and high-resolution Sidi Ali record demonstrates enhanced productivity and lake levels indicating wetter climatic conditions right after the YD arid event at 11.4 ka cal. BP (Zielhofer et al., 2017a). However, the lacustrine records spanning the Late Glacial-Holocene transition generally indicate a shift at the onset of the Holocene (12–11.5 ka cal. BP interval), with higher lake levels (Zielhofer et al., 2017a) or forest development (Rhoujjati et al., 2010; Tabel et al., 2016), rather than reflecting the Atlantic influence with enhanced winter rains.

Regarding the rapid changes described in the wetland formation, the first phase of geomorphic stability (A) is concomitant with the onset of the Sapropel formation in the Eastern Mediterranean, and occurred right before the global increase of wetter climatic conditions in the Alboran Sea (Fig. 13, De Lange et al., 2008; Fletcher and Sanchez-Goñi, 2008). The chronology of the B stability phase is less certain, and care must be taken when interpreting this phase. However, as for phase A, this phase is concomitant with times of winter rain minima, as evidenced by the Middle Atlas rainfall proxy (Ait Brahim et al., 2019). The C and D phases are in good agreement with two wetter periods recorded in the Alboran Sea (Fletcher and Sanchez-Goñi, 2008), with the latter showing an intervening period ca. 9200 cal. BP marked by drier conditions, which is consistent with enhanced flood activity recorded in the Kert and Tabouda rivers, as discussed in section 5.2. Moreover, the D stability phase is also rather coherent with wetter conditions in the Middle and High Atlas (Sha et al., 2019; Zielhofer et al., 2019).

The end of the Moulouya wetland formation in the course of the 6th millennium is in agreement with the end of wet climatic conditions in the AHP records (Shanahan et al., 2015), as well as with the climatic aridification recognised in the western Mediterranean (Fletcher and Zielhofer, 2013). Indeed, at the western Saharan coast, the AHP ended within a few hundred years at around ca. 5.5–5 ka cal. BP (Fig. 13, deMenocal et al., 2000a; McGee et al., 2013). The end of the Moulouya wetland formation is also correlated with the termination of the northern Saharan palaeolakes ca. 6-5 ka BP (Gasse, 2002; Callot and Fontugne, 2008), as well as with an enhanced dust increase in the Sidi Ali record during this 6–5 ka interval, after which a shift in the provenance proxy was noted, reflecting the Mid-Holocene Saharan aridification (Zielhofer et al., 2017b). Jaouadi et al. (2016) highlighted a drop in humidity and an enhanced Saharan dust supply in Tunisia ca. 5.7–4.6 ka cal. BP, whereas Zielhofer and Faust (2008) demonstrate increased flood activity starting from 4.8 ka cal. BP, both of which can be interpreted as a major shift towards aridification. Using a multi-archive comparison, Fletcher and Zielhofer (2013) identified predominant RCC-driven climatic aridity in the western Mediterranean during the 6–5 cal. ka interval. RCCs may play a part in the termination of the Early to Mid-Holocene wet conditions, as cold events are recorded during this interval in the Alboran Sea, such as AC2 or APC4 (Cacho et al., 2001; Combourieu-Nebout et al., 2009), consistent with a long-lasting North Atlantic IRD event ca. 6-5 ka cal. BP (Bond event 4, Bond et al., 2001). Indeed, the transition from wet conditions towards drier conditions that occurred at ca. 6.2 ka cal. BP in the Tabouda floodplain was synchronous with the M6 cold event from the Baleares (Frigola et al., 2007). The 5.1 ka cal. BP reversal in the Blirh floodplain also corresponds to other cold events, such as the M5 event and forest decline (Fig. 13, Frigola et al., 2007; Fletcher and Sanchez-Goñi, 2008). All this evidence suggests a climatic shift towards global aridification of the Mediterranean and North Africa during the 6–5 cal. ka interval, which appears to result in the fluvial tipping point observed in the Tabouda and Blirh Rivers.

6 Conclusion

The alluvial archives from Tabouda and Blirh Rivers, which are representative of the Holocene sedimentary formations from the Ksabi and the Aïn Beni Mathar basins, shed light on the fluvial response of the Moulouya catchment to Early and Late-Holocene climatic changes. Sedimentological, geochemical, and palaeoecological data demonstrate that the fluvial morphogenesis follows a regional pattern controlled by climatic changes. At an orbital scale, the upstream Moulouya fluvial archives record the occurrence of a regional wetland formation between ca. 10.8 to 6-5 cal. ka BP that was not described in other NE Moroccan rivers. At that time, alluvial plains displayed extensive flat organic sedimentary deposits, indicating the development of palustrine environments and tufa sedimentation, sometimes forming tufa dams associated with coexisting marshes and low-energy stream channels. This formation, indicating long-term landscape stability, occurred during the last African Humid Period (AHP), and may be considered a counterpart to the Saharan palaeolakes on the northern side of the High Atlas. Hence, we assume that the Moulouya fluvial and fluvio-palustrine wetland formation located at 32°–34°N is associated with the northern archives recording AHP wet conditions. We also document rapid palaeoenvironmental changes at multi-centennial to millennial scale. Indeed, four particular phases of regional geomorphic stability have been dated to ca. 10800–10500, 10200–9900, 9300, and 8900 cal. BP. Several enhanced flooding periods, reflecting times of climatic aridification, are evidenced and may be related to Early and Mid-Holocene Rapid Climatic Changes. A particular flooding phase is identified at a regional scale which occurred during the 9.2 ka event. Taphonomic conditions, e.g. post-depositional processes, are taken into account, and explain discrepancies in the preservation of fluvial records, notably due to Mid-to-Late Holocene entrenchment of river systems. Indeed, post incision-aggradation coupled processes have removed Early to Mid-Holocene deposits at different times. Finally, this study provides evidence of important morphogenic changes at the end of the Mid-Holocene, such as a probable fluvial tipping point associated with the climatic aridification widely identified in the Mediterranean and North Africa.

7 Acknowledgments

B.D. was supported by a grant from LabEx ARCHIMEDE - ANR-11-LABX-0032-01 -. Fieldwork and analyses were supported by the PALEOMAR program from LabEx ARCHIMEDE, and by the MISTRALS-PaleoMex program, funded by CNRS-INEE (French National Centre for Scientific Research). We deeply thank Dr. Miryam Bar-Matthews (editor) and two anonymous reviewers for their very helpful remarks and suggestions. We also thank Adrien Barra, André-Marie Dendievel, and Laurent Dezileau for their help on the fieldwork. We would also like to thank Karl Embleton for his review of the English version and finally the UMR 5138 Arar and the UMS 2572 LMC14 for ^{14}C measurements in the frame of the ARTEMIS national service and the Poznan Radiocarbon Laboratory.

8 References

Ait Brahim, Y., Wassenburg, J.A., Sha, L., Cruz, F.W., Deininger, M., Sifeddine, A., Bouchaou, L., Spötl, C., Edwards, R.L., Cheng, H., 2019. North Atlantic Ice-Rafting, Ocean and Atmospheric Circulation During the Holocene: Insights From Western Mediterranean Speleothems. Geophysical Research Letters 46, 7614–7623. https://doi.org/10.1029/2019GL082405

Aitchison, J., 1986. The Statistical Analysis of Compositional Data. Chapman & Hall, London.

Aitchison, J., 1982. The Statistical Analysis of Compositional Data. Journal of the Royal Statistical Society: Series B (Methodological) 44, 139–160. https://doi.org/10.1111/j.2517-6161.1982.tb01195.x

Barathon, J.-J., El Abassi, H., Lechevalier, C., Malek, F., Jolly-Saad, M.-C., 2000. Mise au point sur les formations holocènes dans le Rif oriental (Maroc) / A chronology of Holocene deposits in the eastern Rif mountains (Morocco). Géomorphologie : relief, processus, environnement 6, 221–238. https://doi.org/10.3406/morfo.2000.1068

Bartz, M., Rixhon, G., Kehl, M., El Ouahabi, M., Klasen, N., Brill, D., Weniger, G.-C., Mikdad, A., Brückner, H., 2017. Unravelling fluvial deposition and pedogenesis in ephemeral stream deposits in the vicinity of the prehistoric rock shelter of Ifri n'Ammar (NE Morocco) during the last 100 ka. CATENA 152, 115–134. https://doi.org/10.1016/j.catena.2016.12.007

Beck, H.E., Zimmermann, N.E., McVicar, T.R., Vergopolan, N., Berg, A., Wood, E.F., 2018. Present and future Köppen-Geiger climate classification maps at 1-km resolution. Scientific Data 5. https://doi.org/10.1038/sdata.2018.214

Benito, G., Macklin, M.G., Zielhofer, C., Jones, A.F., Machado, M.J., 2015. Holocene flooding and climate change in the Mediterranean. Catena 130, 13–33. https://doi.org/10.1016/j.catena.2014.11.014

Bond, G., Kromer, B., Beer, J., Muscheler, R., Evans, M.N., Showers, W., Hoffmann, S., Lotti-Bond, R., Hajdas, I., Bonani, G., 2001. Persistent Solar Influence on North Atlantic Climate During the Holocene. Science 294, 2130–2136. https://doi.org/10.1126/science.1065680

Bosmans, J.H.C., Drijfhout, S.S., Tuenter, E., Lourens, L.J., Hilgen, F.J., Weber, S.L., 2012. Monsoonal response to mid-holocene orbital forcing in a high resolution GCM. Clim. Past 8, 723–740. https://doi.org/10.5194/cp-8-723-2012

Bouazza, M., Khattach, D., Houari, M.R., Kaufmann, O., 2013. Contribution of the 3D geological model to the study of the Aïn Béni Mathar deep aquifer structure, Eastern Morocco. Bulletin de l'Institut Scientifique 35, 53–61.

Brayshaw, D.J., Rambeau, C.M.C., Smith, S.J., 2011. Changes in Mediterranean climate during the Holocene: Insights from global and regional climate modelling. The Holocene 21, 15–31. https://doi.org/10.1177/0959683610377528

Cacho, I., Grimalt, J.O., Canals, M., Sbaffi, L., Shackleton, N.J., Schönfeld, J., Zahn, R., 2001. Variability of the western Mediterranean Sea surface temperature during the last 25,000 years and its connection with the Northern Hemisphere climatic changes. Paleoceanography 16, 40–52. https://doi.org/10.1029/2000PA000502

Callot, Y., Fontugne, M., 2008. Les sites lacustres d'âge holocène dans l'est du Grand Erg occidental (nord-ouest du Sahara algérien) : interprétation géomorphologique et paléoclimatique. geomorphologie 14, 187–200. https://doi.org/10.4000/geomorphologie.7173

Carrión, J.S., 2002. Patterns and processes of Late Quaternary environmental change in a montane region of southwestern Europe. Quaternary Science Reviews 21, 2047–2066. https://doi.org/10.1016/S0277-3791(02)00010-0

Cheddadi, R., Lamb, H.F., Guiot, J., van der Kaars, S., 1998. Holocene climatic change in Morocco: a quantitative reconstruction from pollen data. Climate Dynamics 14, 883–890. https://doi.org/10.1007/s003820050262

Comas-Cufí, M., Thió-Henestrosa, S., 2011. CoDaPack 2.0: a stand-alone, multi-platform compositional software, in: Egozcue, J.J., Tolosana-Delgado, R., Ortego, M.I. (Eds.), Proceedings of the 4th International Workshop on Compositional Data Analysis. Sant Feliu de Guíxols.

Combourieu Nebout, N., Peyron, O., Dormoy, I., 2009. Rapid climatic variability in the west Mediterranean during the last 25 000 years from high resolution pollen data. Climate of the Past Discussions 5, 671–707. https://doi.org/10.5194/cpd-5-671-2009

Combourieu-Nebout, N., Peyron, O., Bout-Roumazeilles, V., Goring, S., Dormoy, I., Joannin, S., Sadori, L., Siani, G., Magny, M., 2013. Holocene vegetation and climate changes in the central Mediterranean inferred from a high-resolution marine pollen record (Adriatic Sea). Clim. Past 9, 2023–2042. https://doi.org/10.5194/cp-9-2023-2013

Dallmeyer, A., Claussen, M., Lorenz, S.J., Shanahan, T., 2020. The end of the African humid period as seen by a transient comprehensive Earth system model simulation of the last 8000 years. Clim. Past 16, 117–140. https://doi.org/10.5194/cp-16-117-2020

De Lange, G.J., Thomson, J., Reitz, A., Slomp, C.P., Speranza Principato, M., Erba, E., Corselli, C., 2008. Synchronous basin-wide formation and redox-controlled preservation of a Mediterranean sapropel. Nature Geosci 1, 606–610. https://doi.org/10.1038/ngeo283

Dearing, J., 1999. Environmental Magnetic Susceptibility: Using the Bartington MS2 System, second. ed. Chi Publishing, Kenilworth.

deMenocal, P., Ortiz, J., Guilderson, T., Adkins, J., Sarnthein, M., Baker, L., Yarusinsky, M., 2000a. Abrupt onset and termination of the African Humid Period: Quaternary Science Reviews 19, 347–361. https://doi.org/10.1016/S0277-3791(99)00081-5

deMenocal, P., Ortiz, J., Guilderson, T., Sarnthein, M., 2000b. Coherent High- and Low-Latitude Climate Variability During the Holocene Warm Period. Science 288, 2198–2202. https://doi.org/10.1126/science.288.5474.2198

Desprat, S., Combourieu-Nebout, N., Essallami, L., Sicre, M.A., Dormoy, I., Peyron, O., Siani, G., Bout Roumazeilles, V., Turon, J.L., 2013. Deglacial and Holocene vegetation and climatic changes in the southern Central Mediterranean from a direct land–sea correlation. Clim. Past 9, 767–787. https://doi.org/10.5194/cp-9-767-2013

El Amrani, M., Macaire, J.-J., Zarki, H., Bréhéret, J.-G., Fontugne, M., 2008. Contrasted morphosedimentary activity of the lower Kert River (northeastern Morocco) during the Late Pleistocene and the Holocene. Possible impact of bioclimatic variations and human action. Comptes Rendus Geoscience 340, 533–542. https://doi.org/10.1016/j.crte.2008.05.004

El Harradji, A., 1997. Aménagement, érosion et désertification sur les Hauts-Plateaux du Maroc oriental. Méditerranée 86, 15–23. https://doi.org/10.3406/medit.1997.2985

El Harradji, A., 1994. Structuration géologique et évolution géomorphologique du Massif de Debdou (Maroc Oriental). Rev. Géogr. Maroc 16, 127–148.

El Harradji, A., 1985. “Le Massif de Debdou”, Etude géomorphologique (PhD Thesis). Paris I Panthéon-Sorbonne.

Erhart, H., 1955. “Biostasie” et “Rhexistasie”. Esquisse d’une théorie sur le rôle de la pédogénèse en tant que phénomène géologique. C.R. Acad. Sci. Paris 241, 1218–1220.

Esri. "Satellite image" [basemap]. Scale Not Given. "World Imagery", 2009. Accessed 2020-06-05 from http://www.arcgis.com/home/item.html?id=10df2279f9684e4a9f6a7f08febac2a9

Faust, D., Zielhofer, C., Escudero, R.B., del Olmo, F.D., 2004. High-resolution fluvial record of late Holocene geomorphic change in northern Tunisia: climatic or human impact? Quaternary Science Reviews 23, 1757–1775. https://doi.org/10.1016/j.quascirev.2004.02.007

Faust, D., Wolf, D., 2017. Interpreting drivers of change in fluvial archives of the Western Mediterranean - A critical view. Earth-Science Reviews 174, 53–83. https://doi.org/10.1016/j.earscirev.2017.09.011

Fletcher, W.J., Sánchez Goñi, M.F., 2008. Orbital- and sub-orbital-scale climate impacts on vegetation of the western Mediterranean basin over the last 48,000 yr. Quaternary Research 70, 451–464. https://doi.org/10.1016/j.yqres.2008.07.002

Fletcher, W.J., Sanchez Goñi, M.F., Peyron, O., Dormoy, I., 2010. Abrupt climate changes of the last deglaciation detected in a Western Mediterranean forest record. Clim. Past 6, 245–264. https://doi.org/10.5194/cp-6-245-2010

Fletcher, W.J., Zielhofer, C., 2013. Fragility of Western Mediterranean landscapes during Holocene Rapid Climate Changes. Catena 103, 16–29. https://doi.org/10.1016/j.catena.2011.05.001

Fletcher, W.J., Zielhofer, C., Mischke, S., Bryant, C., Xu, X., Fink, D., 2017. AMS radiocarbon dating of pollen concentrates in a karstic lake system. Quaternary Geochronology 39, 112–123. https://doi.org/10.1016/j.quageo.2017.02.006

Fontes, J.Ch., Gasse, F., Callot, Y., Plaziat, J.-C., Carbonel, P., Dupeuble, P.A., Kaczmarska, I., 1985. Freshwater to marine-like environments from Holocene lakes in northern Sahara. Nature 317, 608–610. https://doi.org/10.1038/317608a0

Frigola, J., Moreno, A., Cacho, I., Canals, M., Sierro, F.J., Flores, J.A., Grimalt, J.O., Hodell, D.A., Curtis, J.H., 2007. Holocene climate variability in the western Mediterranean region from a deepwater sediment record: HOLOCENE CLIMATE VARIABILITY. Paleoceanography 22. https://doi.org/10.1029/2006PA001307

Gasse, F., 2002. Diatom-inferred salinity and carbonate oxygen isotopes in Holocene waterbodies of the western Sahara and Sahel (Africa). Quaternary Science Reviews 21, 737–767. https://doi.org/10.1016/S0277-3791(01)00125-1

Gasse, F., 2000. Hydrological changes in the African tropics since the Last Glacial Maximum. Quaternary Science Reviews 19, 189–211. https://doi.org/10.1016/S0277-3791(99)00061-X

Gasse, F., Téhet, R., Durand, A., Gibert, E., Fontes, J.-C., 1990. The arid–humid transition in the Sahara and the Sahel during the last deglaciation. Nature 346, 141–146. https://doi.org/10.1038/346141a0

Heiri, O., Lotter, A.F., Lemcke, G., 2001. Loss on ignition as a method for estimating organic and carbonate content in sediments: reproducibility and comparability of results. Journal of Paleolimnology 25, 101–110. https://doi.org/10.1023/A:1008119611481

Hughes, P.D., Fink, D., Rodés, Á., Fenton, C.R., Fujioka, T., 2018. Timing of Pleistocene glaciations in the High Atlas, Morocco: New 10Be and 36Cl exposure ages. Quaternary Science Reviews 180, 193–213. https://doi.org/10.1016/j.quascirev.2017.11.015

Hylander, L.D., Meili, M., Oliveira, L.J., de Castro e Silva, E., Guimarães, J.R.D., Araujo, D.M., Neves, R.P., Stachiw, R., Barros, A.J.P., Silva, G.D., 2000. Relationship of mercury with aluminum, iron and manganese oxy-hydroxides in sediments from the Alto Pantanal, Brazil. The Science of The Total Environment 260, 97–107. https://doi.org/10.1016/S0048-9697(00)00544-1

Ibouhouten, H., Zielhofer, C., Mahjoubi, R., Kamel, S., Linstädter, J., Mikdad, A., Bussmann, J., Werner, P., Härtling, J.W., Fenech, K., 2010. Archives alluviales holocènes et occupation humaine en Basse Moulouya (Maroc nord-oriental). Géomorphologie : relief, processus, environnement 16, 41–56. https://doi.org/10.4000/geomorphologie.7812

Jaouadi, S., Lebreton, V., Bout-Roumazeilles, V., Siani, G., Lakhdar, R., Boussoffara, R., Dezileau, L., Kallel, N., Mannai-Tayech, B., Combourieu-Nebout, N., 2016. Environmental changes, climate and anthropogenic impact in south-east Tunisia during the last 8 kyr. Clim. Past 12, 1339–1359. https://doi.org/10.5194/cp-12-1339-2016

Jones, A.F., Macklin, M.G., Brewer, P.A., 2012. A geochemical record of flooding on the upper River Severn, UK, during the last 3750years. Geomorphology 179, 89–105. https://doi.org/10.1016/j.geomorph.2012.08.003

Kabata-Pendias, A., 2001. Trace Elements in Soils and Plants, 3rd ed. CRC Press.

Knippertz, P., Wernli, H., 2010. A Lagrangian Climatology of Tropical Moisture Exports to the Northern Hemispheric Extratropics. Journal of Climate 23, 987–1003. https://doi.org/10.1175/2009JCLI3333.1

Kröpelin, S., Verschuren, D., Lézine, A.-M., Eggermont, H., Cocquyt, C., Francus, P., Cazet, J.-P., Fagot, M., Rumes, B., Russell, J.M., Darius, F., Conley, D.J., Schuster, M., von Suchodoletz, H., Engstrom, D.R., 2008. Climate-Driven Ecosystem Succession in the Sahara: The Past 6000 Years. Science 320, 765–768. https://doi.org/10.1126/science.1154913

Lamb, H.F., Gasse, F., Benkaddour, A., El Hamouti, N., van der Kaars, S., Perkins, W.T., Pearce, N.J., Roberts, C.N., 1995. Relation between century-scale Holocene arid intervals in tropical and temperate zones. Nature 373, 134–137. https://doi.org/10.1038/373134a0

Larrasoaña, J.C., Roberts, A.P., Rohling, E.J., 2013. Dynamics of Green Sahara Periods and Their Role in Hominin Evolution. PLoS ONE 8, e76514. https://doi.org/10.1371/journal.pone.0076514

Lefèvre, D., 1985. Les formations plio-pléistocènes du bassin de Ksabi (Moyenne Moulouya, Maroc) (PhD Thesis). Bordeaux 1.

Lefèvre, D., 1989. Formations continentales pléistocenes et paléoenvironnements sédimentaires dans le bassin de Ksabi (Moyenne Moulouya, Maroc). Bulletin de l’Association française pour l’étude du quaternaire 26, 101–113. https://doi.org/10.3406/quate.1989.1897

Lefèvre, D., Ballouche, A., 1991. Evolution des paléoenvironnements de la marge saharienne à l’Holocène : exemple du bassin de Ksabi (Moyenne Moulouya, Maroc)., in: Datations et Caractérisation Des Milieux Pléistocènes, Cahiers Du Quaternaire. CNRS, pp. 451–477.

Lézine, A.-M., Hély, C., Grenier, C., Braconnot, P., Krinner, G., 2011. Sahara and Sahel vulnerability to climate changes, lessons from Holocene hydrological data. Quaternary Science Reviews 30, 3001–3012. https://doi.org/10.1016/j.quascirev.2011.07.006

Limondin-Lozouet, N., Haddoumi, H., Lefèvre, D., Ghamizi, M., Aouraghe, H., Salel, T., 2013. Holocene molluscan succession from NE Morocco:

Palaeoenvironmental reconstruction and biogeographical implications. Quaternary International 302, 61–76. https://doi.org/10.1016/j.quaint.2012.11.036

Magny, M., Combourieu-Nebout, N., de Beaulieu, J.L., Bout-Roumazeilles, V., Colombaroli, D., Desprat, S., Francke, A., Joannin, S., Ortu, E., Peyron, O., Revel, M., Sadori, L., Siani, G., Sicre, M.A., Samartin, S., Simonneau, A., Tinner, W., Vannière, B., Wagner, B., Zanchetta, G., Anselmetti, F., Brugiapaglia, E., Chapron, E., Debret, M., Desmet, M., Didier, J., Essallami, L., Galop, D., Gilli, A., Haas, J.N., Kallel, N., Millet, L., Stock, A., Turon, J.L., Wirth, S., 2013. North-south palaeohydrological contrasts in the central Mediterranean during the Holocene: tentative synthesis and working hypotheses. Clim. Past 9, 2043–2071. https://doi.org/10.5194/cp-9-2043-2013

Magny, M., Vannière, B., Calo, C., Millet, L., Leroux, A., Peyron, O., Zanchetta, G., La Mantia, T., Tinner, W., 2011. Holocene hydrological changes in south-western Mediterranean as recorded by lake-level fluctuations at Lago Preola, a coastal lake in southern Sicily, Italy. Quaternary Science Reviews 30, 2459–2475. https://doi.org/10.1016/j.quascirev.2011.05.018

McGee, D., deMenocal, P.B., Winckler, G., Stuut, J.B.W., Bradtmiller, L.I., 2013. The magnitude, timing and abruptness of changes in North African dust deposition over the last 20,000yr. Earth and Planetary Science Letters 371–372, 163–176. https://doi.org/10.1016/j.epsl.2013.03.054

McLennan, S.M., Murray, R.W., 1999. Geochemistry of sediments, in: Marshall, C.P., Fairbridge, R.W. (Eds.), Encyclopedia of Geochemistry. Kluwer Academic Publishers, Dordrecht, pp. 282–292.

Médioni, R., 1960. Contribution à l’étude géologique des Hauts Plateaux méridionaux marocains. Notes du Service géologique du Maroc 19, 7–53.

Michard, A., Saddiqi, O., Chalouan, A., Lamotte, D.F. de (Eds.), 2008. Continental Evolution: The Geology of Morocco: Structure, Stratigraphy, and Tectonics of the Africa-Atlantic-Mediterranean Triple Junction, Lecture Notes in Earth Sciences. Springer Berlin Heidelberg, Berlin, Heidelberg. https://doi.org/10.1007/978-3-540-77076-3

Mihaljevic, M., 1999. Zinc, in: Marshall, C.P., Fairbridge, R.W. (Eds.), Encyclopedia of Geochemistry. Kluwer Academic Publishers, Dordrecht, pp. 674–675.

NASA/METI/AIST/Japan Spacesystems, and U.S./Japan ASTER Science Team, 2009. ASTER Global Digital Elevation Model [Data set]. NASA EOSDIS Land Processes DAAC. Accessed 2020-06-05 from https://doi.org/10.5067/ASTER/ASTGTM.002

Nour El Bait, M., Rhoujjati, A., Eynaud, F., Benkaddour, A., Dezileau, L., Wainer, K., Goslar, T., Khater, C., Tabel, J., Cheddadi, R., 2014. An 18 000-year pollen and sedimentary record from the cedar forests of the Middle Atlas, Morocco: POLLEN/SEDIMENTARY RECORD FROM THE MIDDLE ATLAS. Journal of Quaternary Science 29, 423–432. https://doi.org/10.1002/jqs.2708

Pausata, F.S.R., Messori, G., Zhang, Q., 2016. Impacts of dust reduction on the northward expansion of the African monsoon during the Green Sahara period. Earth and Planetary Science Letters 434, 298–307. https://doi.org/10.1016/j.epsl.2015.11.049

Petrie, L.M., 1999. Manganese, in: Marshall, C.P., Fairbridge, R.W. (Eds.), Encyclopedia of Geochemistry. Kluwer Academic Publishers, Dordrecht, pp. 382–384.

Peyron, O., Combourieu-Nebout, N., Brayshaw, D., Goring, S., Andrieu-Ponel, V., Desprat, S., Fletcher, W., Gambin, B., Ioakim, C., Joannin, S., Kotthoff, U., Kouli, K., Montade, V., Pross, J., Sadori, L., Magny, M., 2017. Precipitation changes in the Mediterranean basin during the Holocene from terrestrial and marine pollen records: a model–data comparison. Clim. Past 13, 249–265. https://doi.org/10.5194/cp-13-249-2017

Profe, J., Zolitschka, B., Schirmer, W., Frechen, M., Ohlendorf, C., 2016. Geochemistry unravels MIS 3/2 paleoenvironmental dynamics at the loess–paleosol sequence Schwalbenberg II, Germany. Palaeogeography, Palaeoclimatology, Palaeoecology 459, 537–551. https://doi.org/10.1016/j.palaeo.2016.07.022

Puisségur, J.J., 1976. Mollusques continentaux quaternaires de Bourgogne, Mémoires Géologiques de l’Université de Dijon 3. Doin, Paris.

Reimer, P.J., Austin, W.E.N., Bard, E., Bayliss, A., Blackwell, P.G., Bronk Ramsey, C., Butzin, M., Cheng, H., Edwards, R.L., Friedrich, M., Grootes, P.M., Guilderson, T.P., Hajdas, I., Heaton, T.J., Hogg, A.G., Hughen, K.A., Kromer, B., Manning, S.W., Muscheler, R., Palmer, J.G., Pearson, C., van der Plicht, J., Reimer, R.W., Richards, D.A., Scott, E.M., Southon, J.R., Turney, C.S.M., Wacker, L., Adolphi, F., Büntgen, U., Capano, M., Fahrni, S.M., Fogtmann-Schulz, A., Friedrich, R., Köhler, P., Kudsk, S., Miyake, F., Olsen, J., Reinig, F., Sakamoto, M., Sookdeo, A., Talamo, S., 2020. The IntCal20 Northern Hemisphere Radiocarbon Age Calibration Curve (0–55 cal kBP). Radiocarbon 62, 725–757. https://doi.org/10.1017/RDC.2020.41

Revel, M., Ducassou, E., Grousset, F.E., Bernasconi, S.M., Migeon, S., Revillon, S., Mascle, J., Murat, A., Zaragosi, S., Bosch, D., 2010. 100,000 Years of African monsoon variability recorded in sediments of the Nile margin. Quaternary Science Reviews 29, 1342–1362. https://doi.org/10.1016/j.quascirev.2010.02.006

Rhoujjati, A., Cheddadi, R., Taïeb, M., Baali, A., Ortu, E., 2010. Environmental changes over the past c. 29,000 years in the Middle Atlas (Morocco): A record from Lake Ifrah. Journal of Arid Environments 74, 737–745. https://doi.org/10.1016/j.jaridenv.2009.09.006

Robinson, G.D., 1981. Adsorption of Cu, Zn and Pb near sulfide deposits by hydrous manganese—Iron oxide coatings on stream alluvium. Chemical Geology 33, 65–79. https://doi.org/10.1016/0009-2541(81)90085-1

Rohling, E.J., Marino, G., Grant, K.M., 2015. Mediterranean climate and oceanography, and the periodic development of anoxic events (sapropels). Earth-Science Reviews 143, 62–97. https://doi.org/10.1016/j.earscirev.2015.01.008

Rothwell, R.G., Croudace, I.W., 2015. Twenty Years of XRF Core Scanning Marine Sediments: What Do Geochemical Proxies Tell Us?, in: Croudace, I.W., Rothwell, R.G. (Eds.), Micro-XRF Studies of Sediment Cores: Applications of a Non-Destructive Tool for the Environmental Sciences, Developments in Paleoenvironmental Research. Springer Netherlands, Dordrecht, pp. 25–102.

Sancho, C., Peña, J.L., Muñoz, A., Benito, G., McDonald, E., Rhodes, E.J., Longares, L.A., 2008. Holocene alluvial morphopedosedimentary record and environmental changes in the Bardenas Reales Natural Park (NE Spain). Catena 73, 225–238. https://doi.org/10.1016/j.catena.2007.09.011

Sebbar, A., 2013. Etude de la variabilité et de l’évolution de la pluviométrie au Maroc (1935-2005): Réactualisation de la carte des précipitations (PhD Thesis). Hassan II Mohammedia, Casablanca.

Sha, L., Ait Brahim, Y., Wassenburg, J.A., Yin, J., Peros, M., Cruz, F.W., Cai, Y., Li, H., Du, W., Zhang, H., Edwards, R.L., Cheng, H., 2019. How Far North Did the African Monsoon Fringe Expand During the African Humid Period? Insights From Southwest Moroccan Speleothems. Geophys. Res. Lett. 46, 14093–14102. https://doi.org/10.1029/2019GL084879

Shanahan, T.M., McKay, N.P., Hughen, K.A., Overpeck, J.T., Otto-Bliesner, B., Heil, C.W., King, J., Scholz, C.A., Peck, J., 2015. The time-transgressive termination of the African Humid Period. Nature Geoscience 8, 140–144. https://doi.org/10.1038/ngeo2329

Stretta, E., 1952. Etude hydrogéologique du bassin de l'Oued El Haï (Hauts Plateaux du Maroc oriental), Notes et Mémoires. Service géologique du Maroc, Rabat.

Tabel, J., Khater, C., Rhoujjati, A., Dezileau, L., Bouimetarhan, I., Carre, M., Vidal, L., Benkaddour, A., Nourelbait, M., Cheddadi, R., 2016. Environmental changes over the past 25 000 years in the southern Middle Atlas, Morocco: PAST ENVIRONMENTAL CHANGES IN MOROCCO. Journal of Quaternary Science 31, 93–102. https://doi.org/10.1002/jqs.2841

Thornes, J., López-Bermúdez, F., Woodward, J., 2009. Hydrology, river regimes and sediment yield, in: Woodward, J. (Ed.), The Physical Geography of the Mediterranean. Oxford University Press, Oxford, pp. 229–253.

Tierney, J.E., Pausata, F.S.R., deMenocal, P.B., 2017. Rainfall regimes of the Green Sahara. Science Advances 3, e1601503. https://doi.org/10.1126/sciadv.1601503

Vacchi, M., Marriner, N., Morhange, C., Spada, G., Fontana, A., Rovere, A., 2016. Multiproxy assessment of Holocene relative sea-level changes in the western Mediterranean: Sea-level variability and improvements in the definition of the isostatic signal. Earth-Science Reviews 155, 172–197. https://doi.org/10.1016/j.earscirev.2016.02.002

Walker, M., Head, M.J., Berkelhammer, M., Björck, S., Cheng, H., Cwynar, L., Fisher, D., Gkinis, V., Long, A., Lowe, J., Newnham, R., Rasmussen, S.O., Weiss, H., 2018. Formal ratification of the subdivision of the Holocene Series/Epoch (Quaternary System/Period): two new Global Boundary Stratotype Sections and Points (GSSPs) and three new stages/subseries. Episodes 41, 213–223. https://doi.org/10.18814/epiiugs/2018/018016

Wang, M., Zheng, H., Xie, X., Fan, D., Yang, S., Zhao, Q., Wang, K., 2011. A 600-year flood history in the Yangtze River drainage: Comparison between a subaqueous delta and historical records. Chin. Sci. Bull. 56, 188–195. https://doi.org/10.1007/s11434-010-4212-2

Wassenburg, J.A., Dietrich, S., Fietzke, J., Fohlmeister, J., Jochum, K.P., Scholz, D., Richter, D.K., Sabaoui, A., Spötl, C., Lohmann, G., Andreae, M.O., Immenhauser, A., 2016. Reorganization of the North Atlantic Oscillation during early Holocene deglaciation. Nature Geoscience 9, 602–605. https://doi.org/10.1038/ngeo2767

Weldeab, S., Menke, V., Schmiedl, G., 2014. The pace of East African monsoon evolution during the Holocene: WELDEAB ET. AL.; EAST AFRICAN MONSOON EVOLUTION. Geophys. Res. Lett. 41, 1724–1732. https://doi.org/10.1002/2014GL059361

Wengler, L., Vernet, J.-L., 1992. Vegetation, sedimentary deposits and climates during the Late Pleistocene and Holocene in eastern Morocco. Palaeogeography, Palaeoclimatology, Palaeoecology 94, 141–167. https://doi.org/10.1016/0031-0182(92)90117-N

Wengler, L., Vernet, J.-L., Ballouche, A., Damblon, F., Michel, P., 1992. Signification dee paléomilieux et évolution du climat au Maghreb. Le Maroc oriental au Pléistocène récent. Bulletin de la Société Botanique de France. Actualités Botaniques 139, 507–529. https://doi.org/10.1080/01811789.1992.10827124

Wengler, L., Vernet, J.L., Michel, P., 1994. Evénements et chronologie de l'Holocène en milieu continental au Maghreb. Les données du Maroc oriental . [Holocene events and chronology in the continental environment of the Maghreb. Data from eastern Morocco]. Quaternaire 5, 119–134. https://doi.org/10.3406/quate.1994.2023

Wolf, D., Faust, D., 2015. Western Mediterranean environmental changes: Evidences from fluvial archives. Quaternary Science Reviews 122, 30–50. https://doi.org/10.1016/j.quascirev.2015.04.016

Zielhofer, C., Bussmann, J., Ibouhouten, H., Fenech, K., 2010. Flood frequencies reveal Holocene rapid climate changes (Lower Moulouya River, northeastern Morocco). Journal of Quaternary Science 25, 700–714. https://doi.org/10.1002/jqs.1347

Zielhofer, C., Faust, D., 2008. Mid- and Late Holocene fluvial chronology of Tunisia. Quaternary Science Reviews 27, 580–588. https://doi.org/10.1016/j.quascirev.2007.11.019

Zielhofer, C., Faust, D., Escudero, R.B., del Olmo, F.D., Kadereit, A., Moldenhauer, K.-M., Porras, A., 2004. Centennial-scale late-Pleistocene to mid-Holocene synthetic profile of the Medjerda Valley, northern Tunisia. The Holocene 14, 851–861. https://doi.org/10.1191/0959683604hl765rp

Zielhofer, C., Fletcher, W.J., Mischke, S., De Batist, M., Campbell, J.F.E., Joannin, S., Tjallingii, R., El Hamouti, N., Junginger, A., Stele, A., Bussmann, J., Schneider, B., Lauer, T., Spitzer, K., Strupler, M., Brachert, T., Mikdad, A., 2017a. Atlantic forcing of Western Mediterranean winter rain minima during the last 12,000 years. Quaternary Science Reviews 157, 29–51. https://doi.org/10.1016/j.quascirev.2016.11.037

Zielhofer, C., Köhler, A., Mischke, S., Benkaddour, A., Mikdad, A., Fletcher, W.J., 2019. Western Mediterranean hydro-climatic consequences of Holocene ice-rafted debris (Bond) events. Climate of the Past 15, 463–475. https://doi.org/10.5194/cp-15-463-2019

Zielhofer, C., von Suchodoletz, H., Fletcher, W.J., Schneider, B., Dietze, E., Schlegel, M., Schepanski, K., Weninger, B., Mischke, S., Mikdad, A., 2017b. Millennial-scale fluctuations in Saharan dust supply across the decline of the African Humid Period. Quaternary Science Reviews 171, 119–135. https://doi.org/10.1016/j.quascirev.2017.07.010

Zolitschka, B., Rolf, C., Bittmann, F., Binot, F., Frechen, M., Wonik, T., Froitzheim, N., Ohlendorf, C., 2014. Pleistocene climatic and environmental variations inferred from a terrestrial sediment record – the Rodderberg Volcanic Complex near Bonn, Germany. Zeitschrift der Deutschen Gesellschaft für Geowissenschaften 165, 407–424. https://doi.org/10.1127/1860-1804/2014/0071